JOURNAL OF PETROLOGY | VOLUME 41 | NUMBER 8 | PAGES 1271–1305 | 2000

Flood Basalts of Vestfjella: Jurassic Magmatism Across an Archaean–Proterozoic Lithospheric Boundary in Dronning Maud Land, Antarctica

ARTO V. LUTTINEN[1]* AND HARALD FURNES[2]

[1]DEPARTMENT OF GEOLOGY, UNIVERSITY OF HELSINKI, P.O. BOX 11, FIN-00014 HELSINKI, FINLAND

[2]GEOLOGICAL INSTITUTE, UNIVERSITY OF BERGEN, ALLEGT. 41, 5007 BERGEN, NORWAY

RECEIVED FEBRUARY 10, 1999; REVISED TYPESCRIPT ACCEPTED DECEMBER 14, 1999

Continental flood basalts (CFBs) of Jurassic age make up the Vestfjella mountains of western Dronning Maud Land and demonstrate an Antarctic extension of the Karoo large igneous province. A detailed geochemical study of the 120-km-long Vestfjella range shows the CFB suite to consist mainly of three intercalated basaltic rock types designated CT1, CT2 and CT3 (chemical types 1, 2 and 3) that exhibit different incompatible trace element ratios. CT1 and CT2 of north Vestfjella record wide ranges of Nd and Sr isotopic compositions with initial ε_{Nd} and ε_{Sr} ranging from $+7{\cdot}6$ to $-16{\cdot}0$ and -16 to $+65$, respectively. The southern Vestfjella is dominated by CT3 with near-chondritic ε_{Nd} ($+2{\cdot}0$ to $-4{\cdot}1$) and ε_{Sr} (-11 to $+19$). A volumetrically minor suite of ocean island basalt (OIB-)like CT4 dykes (ε_{Nd} $+3{\cdot}6$, ε_{Sr} $+1$) cuts the lava sequence in north Vestfjella. The pronounced isotopic differences suggest different magmatic plumbing systems for the heterogeneous CT1 and CT2 suites and the relatively homogeneous CT3 lavas. This is further supported by the palaeoflow directions, which point to major source regions to the north (CT1 and CT2) and east (CT3) of Vestfjella. These source regions can be associated with two contemporaneous major lithospheric thinning zones that permitted magma emplacement and controlled the melting of upper-mantle sources in the Jurassic Dronning Maud Land. The CT1 and CT2 magmas utilized the northern zone of thinning and were emplaced into the 3 Ga Grunehogna craton, whereas the CT3 magmas were emplaced through thinned Proterozoic Maud Belt lithosphere. Trace element and isotopic studies of the identified magma types reveal a complex history of fractionation and contamination at different lithospheric levels. All extrusive rock types show evidence of crustal contamination but this had rather small impact on their diagnostic trace element ratios. Much stronger overprint, in the CT1 and CT2 suites, resulted from contamination with veined Archaean lithospheric mantle, which produced wide ranges of isotopic and highly incompatible element ratios. CT3, in turn, does not show evidence of interaction with the Proterozoic lithospheric mantle. The high-ε_{Nd} endmembers of CT1, CT2 and CT3 probably closely resemble uncontaminated mantle-derived magmas and indicate three different mantle sources. The CT2 primary magmas were derived from light rare earth element (LREE)-depleted, slightly large ion lithophile element (LILE)-enriched sources, whereas data on the volumetrically preponderant CT1 and CT3 point to variably LREE-enriched, strongly LILE-enriched sources. The sources of CT1, CT2 and CT3 may record large-scale lateral heterogeneity generated by subduction-contamination of the Gondwanan upper mantle. The OIB-like CT4 dykes probably reflect asthenospheric heterogeneities that were unrelated to the proposed subduction-contamination.

KEY WORDS: *Karoo magmatism; Vestfjella (Dronning Maud Land, Antarctica); Sr and Nd isotopes; magmatic differentiation; depleted and enriched mantle sources*

INTRODUCTION

Among the fundamental questions pertaining to the generation of continental flood basalt (CFB) provinces are the importance of crustal contamination and lithospheric

*Corresponding author. e-mail: arto.luttinen@helsinki.fi

Extended data set can be found at: http://www.petrology.oupjournals.org

mantle sources and the relationships between rifting and magmatism. In contrast to the widely supported plume origin for the Mesozoic Karoo magmatism in Africa and Antarctica (Fig. 1) (e.g. Cox, 1989; White & McKenzie, 1989), the great majority of the Karoo basalts exhibit negative initial ε_{Nd}, positive initial ε_{Sr}, and distinct crust-like trace element characteristics—the so-called lithospheric signature (Erlank, 1984). Whereas a crustal origin has been repeatedly suggested for the lithospheric signatures of these and many other CFBs (e.g. Arndt *et al.*, 1993; Chesley & Ruiz, 1998), the bulk of Karoo magmatism has been generally ascribed to enriched lithospheric mantle sources (e.g. Duncan *et al.*, 1984; Hawkesworth *et al.*, 1984; Sweeney *et al.*, 1994). On the other hand, lithospheric mantle has also been considered as a potential contaminant of the Karoo basalts (Ellam & Cox, 1991; Ellam *et al.*, 1992).

Another problematic issue of Karoo volcanism and the Gondwana break-up magmatism in general is the role of subduction processes, previous and contemporaneous, which could have produced enriched upper-mantle sources or otherwise influenced magma generation (e.g. Cox, 1978; Elliot, 1990; Hergt *et al.*, 1991; Brewer *et al.*, 1992; Storey *et al.*, 1992). Considerable ambiguity also surrounds the nature of plume–lithosphere interactions and the causal relationship between magmatism and continental rifting (Sweeney & Watkeys, 1990; Griffiths & Campbell, 1991; Thompson & Gibson, 1991; Cox, 1992; Saunders *et al.*, 1992; White, 1992; Grantham, 1996; Ebinger & Sleep, 1998; Leitch *et al.*, 1998).

The Jurassic CFBs of western Dronning Maud Land, Antarctica, have been viewed as a part of the Karoo large igneous province (e.g. Faure *et al.*, 1979; Harris *et al.*, 1990; Luttinen & Siivola, 1997) (Fig. 1). This paper is an extension of our previous work on the Vestfjella CFB suite (Furnes & Mitchell, 1978; Furnes *et al.*, 1982, 1987; Luttinen & Siivola, 1997; Luttinen *et al.*, 1998). Geochemical studies by Furnes and his coworkers on southern Vestfjella CFBs during the 1980s revealed a heterogeneous suite of lavas and dykes that differ from other Jurassic basalts of western Dronning Maud Land [see also Harris *et al.* (1990)]. On the basis of detailed sampling of two sections (Basen and Plogen; Fig. 1), Luttinen & Siivola (1997) were able to recognize three chemically different basaltic magma series in north Vestfjella and designated them chemical types 1, 2 and 3 (CT1, CT2 and CT3, respectively). Geochemical comparison established an affinity to the Karoo magmatism of the Lebombo Monocline area, notably to Southern Lebombo low-Ti tholeiites by CT1 and to mid-ocean ridge basalt (MORB)-like Rooi Rand dolerites and their extrusive equivalents by CT2. Subsequently, Nd and Sr isotopic data for these rocks were reported by Luttinen *et al.* (1998), who also discovered a minor subgroup of dyke rocks (CT4) and suggested that the heterogeneous CFB magmatism recorded in north Vestfjella had been fundamentally linked to lithospheric mantle sources.

Here we report 210 new chemical and 27 Nd and Sr isotopical analyses of CFBs throughout the 120-km-long Vestfjella range. Combining these with the previously published data, we assess the spatial and temporal relationships between the various magma types on a regional scale. The existing data now cover the Vestfjella suite in considerable detail and enable us to better evaluate the processes that were responsible for generating an exceptionally heterogeneous CFB suite. We examine the magmatic history of each chemical type and evaluate the significance of crustal and lithospheric mantle level contamination and heterogeneous upper-mantle sources. Finally, we propose a tectono-magmatic model that links the origin of the Vestfjella CFBs to several magmatic plumbing systems and active zones of lithospheric thinning in western Dronning Maud Land during the Jurassic.

GEOLOGICAL SETTING

Mesozoic flood lavas crop out at three main localities in Dronning Maud Land: Vestfjella, Kirwanveggen and Heimefrontfjella (Fig. 1). Volumetrically, the most significant lava suites are found in Vestfjella and southern Kirwanveggen. Intrusive equivalents of the flood lavas are abundant in Vestfjella but rare elsewhere. In the Ahlmannryggen–Sverdrupfjella region, however, Mesozoic basaltic lavas are absent but dolerites fairly abundant (Harris *et al.*, 1991).

In Vestfjella, the thickness of the lava pile exceeds 900 m in the north and 400 m in the south. The lavas show an overall W–SW tilt with dips generally $<10°$ (Furnes *et al.*, 1987; Luttinen & Siivola, 1997). The lava pile is cut by dolerite dykes and sills and, at Muren and Utpostane, by gabbro intrusions (Hjelle & Winsnes, 1972; Räisänen *et al.*, 1999). Normal faulting is associated with the dykes and probably was related to dyke emplacement (Spaeth, 1987). The age of the Vestfjella sequence is not accurately constrained. Available K–Ar age data for bulk rocks show large variations, with the majority of the dyke rocks yielding 160–170 Ma, and the lavas 170–230 Ma (Furnes & Mitchell, 1978; Furnes *et al.*, 1987; Peters *et al.*, 1991). The wide range of ages probably reflects subsolidus alteration. Plagioclase K–Ar ages of $\sim$180 Ma for north Vestfjella lavas (Peters *et al.*, 1991) provide the best age estimate available and correspond to a recently obtained $^{39}Ar/^{40}Ar$ age of 183 $\pm$ 1 Ma for basalts in Kirwanveggen and southeast Africa (Duncan *et al.*, 1997).

The base of the lava pile is not exposed in Vestfjella. Elsewhere, the Dronning Maud Land lavas were erupted on a Palaeozoic continental sedimentary sequence overlying a Precambrian basement (Aucamp *et al.*, 1972;

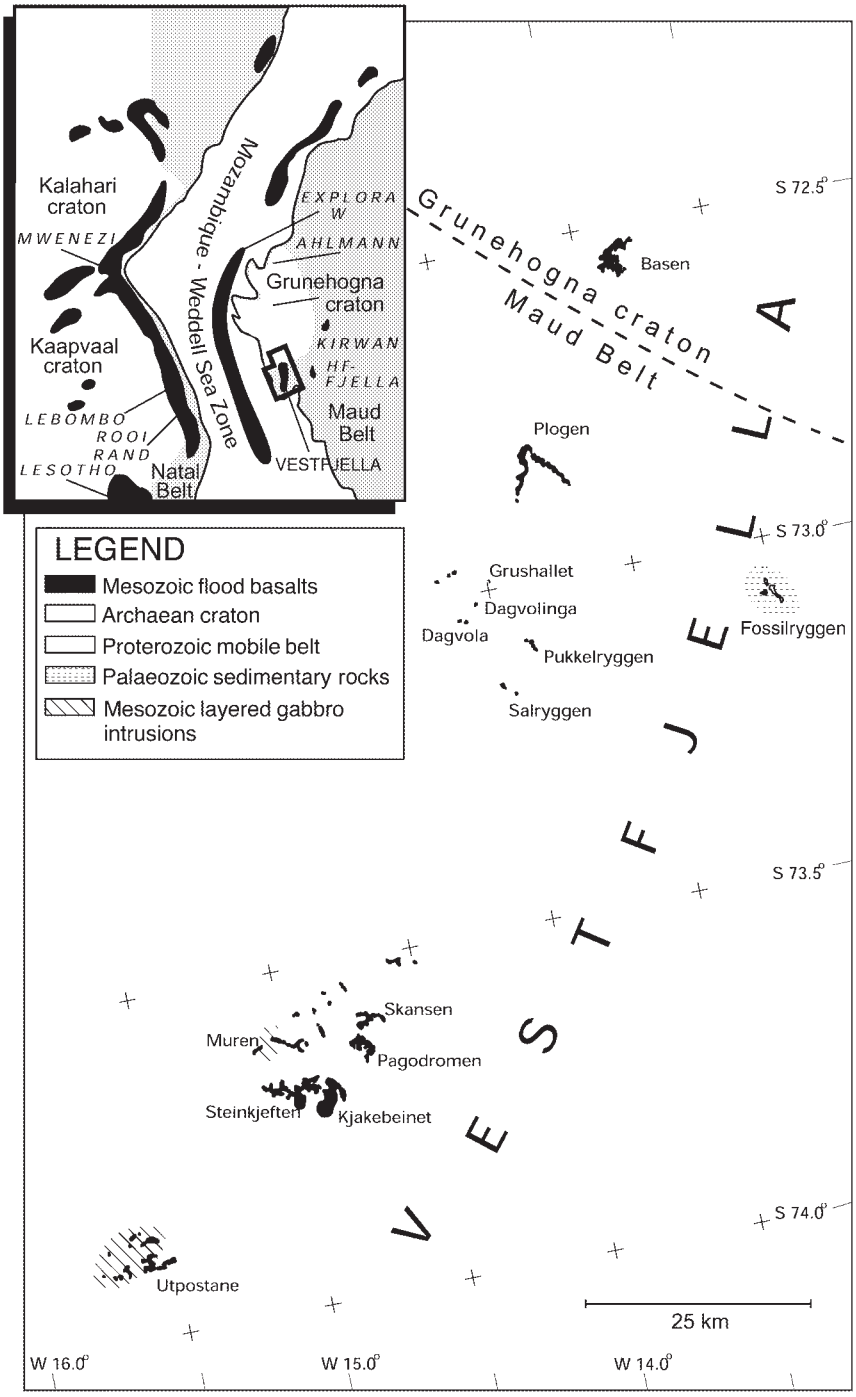

Fig. 1. Distribution of Karoo and related flood basalts and the main lithospheric domains in a schematic Mesozoic Gondwana reconstruction of Africa and Antarctica (inset) and distribution of Mesozoic flood basalts and related gabbro intrusions in Vestfjella, western Dronning Maud Land, Antarctica. Abbreviations for Kirwanveggen, Heimefrontfjella and Ahlmannryggen are Kirwan, HF-Fjella and Ahlmann, respectively. Gondwana reconstruction and Mozambique–Weddell Sea lithospheric thinning zone after Cox (1992).

Hjelle & Winsnes, 1972). The basement is divided into two major domains. Before Mesozoic break-up, the Archaean Grunehogna craton (Halpern, 1970) was probably part of the Kaapvaal craton (Groenewald *et al.*, 1995; Fig. 1). The craton is bounded to the east and southeast by the Mesoproterozoic Maud Belt, the Antarctic

extension of the Natal Belt of Africa (e.g. Jacobs *et al.*, 1993) (Fig. 1). The exact position of the Archaean–Proterozoic lithospheric terrane boundary is not firmly established, but, on the basis of gravity and aeromagnetic data, it has been interpreted to be located within 72°–73°S, i.e. close to north Vestfjella (Corner, 1994; Fig. 1).

Volumetrically, an important part of the Karoo magmatism is represented by the opposing sequences of volcanic rocks of the Lebombo Monocline and the western part of the Explora Wedge (Cox, 1992; Fig. 1). It has been proposed that the generation of these basalt suites was related to development of a major lithospheric thinning zone and the initial opening stage of the Southwest Indian Ocean (e.g. Marsh, 1987; Cox, 1992; Duncan *et al.*, 1997). The southward extension of this so-called Mozambique lithospheric thinning zone (Cox, 1992) followed the present Weddell Sea margin of Dronning Maud Land and could have been petrogenetically linked to the seaward dipping basalt succession of Vestfjella (Fig. 1).

DATASET AND ANALYTICAL METHODS

The 210 samples reported in this study have been collected by the authors during five Norwegian and Finnish Antarctic expeditions during the period 1985–1998 from the localities indicated in Fig. 1. The analysed basalts include one sill rock sample (P27-AVL). The samples were analysed by X-ray fluorescence spectrometry (XRF) for major and trace elements at the Geoanalytical Laboratory, Washington State University (120 samples) and the University of Bergen (90 samples). The analytical procedures used at the Geoanalytical Laboratory are summarized below. For the XRF procedure used in the University of Bergen, the reader is referred to Furnes *et al.* (1996).

The major and minor oxides and Ni, Cr, Sc, V, Ba, Zr, Y, Cu and Zn were analysed by XRF (Rigaku 3370) using the procedure described by Johnson *et al.* (1999). A set of 26 duplicate samples were first analysed at Bergen and then at the Geoanalytical Laboratory to evaluate interlaboratory bias (Appendix, available on the *Journal of Petrology* web site at http://www.petrology.oupjournals.org). Rock chips were pulverized in a tungsten carbide swing mill. The duplicate samples (labelled VF in Table 1) were ground in an agate chamber. The reported precision of analyses is better than 2% for most oxides and trace elements, whereas that for Ni, Cr, Sc and V is better than 10% and that of Cu is better than 18% (Johnson *et al.*, 1999).

A subset of representative samples for isotopic and high-resolution trace element analyses was selected on the basis of the XRF data. Inductively coupled plasma mass spectrometry (ICP-MS) was used for analysis of the lanthanides, Rb, Sr, Nb, Hf, Ta, U, Pb and Th at the Geoanalytical Laboratory. The analytical procedure has been described in detail by Knaack *et al.* (1994). Chips of crushed samples were ground in an iron bowl using a shatter-box swing mill, apart from samples labelled VF (see Table 1), which were pulverized in an agate chamber. The statistics for a single sample (BCR-P) run over a 4 month period indicate that precision for the lanthanides, Rb, Sr, Nb and Hf is better than 2·5%. Precision for Ta and Pb is better than 3·5%, and for Th and U it is better than 10% (Knaack *et al.*, 1994).

Strontium and neodymium isotopes were analysed mainly on a Finnigan 262 mass spectrometer at the University of Bergen. All chemical processing was carried out in a clean-room environment with high efficiency particulate air (HEPA) filtered air supply and positive pressure, and the reagents were purified in two-bottle Teflon stills. Samples were dissolved in a mixture of HF and HNO_3. Strontium was separated by specific extraction chromatography using the method described by Pin *et al.* (1994) and was loaded on a double filament and analysed in static mode. The Sr isotopic ratios were corrected for mass fractionation using a $^{88}Sr/^{86}Sr$ value of 8·375209. Repeated measurements of the NBS 987 Sr standard yielded an average $^{87}Sr/^{86}Sr$ value of $0{\cdot}710251 \pm 19$ (2σ) ($n = 27$).

Rare earth elements (REE) were separated by specific extraction chromatography using the method described by Pin *et al.* (1994). Neodymium was subsequently separated using low-pressure ion-exchange chromatography with di(2-ethylhexyl)orthophosphoric acid (HDEHP)-coated Teflon powder as the ion-exchange resin (Richard *et al.*, 1976) and then loaded on a double filament and analysed in static mode. Nd isotopic ratios were corrected for mass fractionation using a $^{146}Nd/^{144}Nd$ value of 0·7219. Repeated measurements of the JM Nd-standard yielded an average $^{143}Nd/^{144}Nd$ value of $0{\cdot}511113 \pm 15$ (2σ) ($n = 62$).

Two of the samples (P27-AVL and P55-AVL) were analysed for Nd, Sm, Rb and Sr concentrations and isotopic ratios at the Geological Survey of Finland. For analytical methods, the reader is referred to Luttinen *et al.* (1998).

PETROGRAPHY

The chemically analysed samples are typical tholeiitic CFBs. Most of the rocks are porphyritic (83%). The predominant phenocryst assemblages in the order of appearance are: plagioclase (29% of the porphyritic samples), plagioclase + augite (28%), plagioclase + olivine (12%) and plagioclase + augite + olivine (11%).

Table 1: Geochemical data of Mesozoic flood basalts in Vestfjella, Dronning Maud Land, Antarctica

Sample:	VF57-85	P11-AVL	P2-AVL	P23-AVL	P40-AVL	P42-AVL	P59-AVL	P69-AVL	VF76-85	VF80-85	UP206-AVL	SK224-AVL	P37-AVL	P44-AVL	P45-AVL	VF147-85	VF26-85	VF30-85	VF40-85	VF44-85	VF46-85	VF81-85	P55-AVL	B33-AVL	B67-AVL	P18-AVL
Type:*	CT1	CT1	CT1	CT1	CT1	CT1	CT1	CT1	CT1	CT1	CT1	CT1	CT1	CT1	CT1	CT1	CT1	CT1	CT1	CT1	CT1	CT1	CT2	CT2	CT2	CT2
Location:	B	P	P	P	P	P	P	P	P	P	UP	SK	P	P	P	KB	PR	PR	SR	SR	SR	PD	P	B	B	P
Major and minor elements (wt %)†																										
SiO_2	53·36	53·81	52·30	55·32	52·16	52·52	53·14	54·13	55·29	54·77	51·51	53·91	53·27	53·21	53·84	54·32	52·75	53·27	53·56	53·57	53·21	53·15	52·78	54·54	50·68	53·23
TiO_2	1·38	1·13	0·89	0·97	1·03	1·26	0·95	1·05	1·24	1·13	1·63	1·47	1·43	1·53	1·49	1·42	1·56	1·46	1·45	1·57	1·51	1·50	2·18	2·40	3·46	2·56
Al_2O_3	14·97	14·92	12·15	14·62	16·87	15·12	14·89	14·78	14·48	14·75	14·54	15·19	15·05	14·87	15·14	14·94	15·08	15·58	14·73	14·86	14·85	15·12	12·71	13·35	13·13	13·30
FeO_{tot}	9·71	10·00	9·62	8·99	8·83	10·40	9·50	9·67	9·95	9·52	11·69	9·12	10·28	10·38	9·77	9·67	10·43	10·96	10·40	10·23	10·75	10·07	11·26	11·95	14·56	13·28
MnO	0·17	0·16	0·16	0·15	0·14	0·17	0·16	0·17	0·17	0·16	0·19	0·17	0·17	0·17	0·17	0·17	0·18	0·19	0·17	0·17	0·17	0·18	0·17	0·16	0·17	0·17
MgO	5·99	7·30	12·16	8·97	6·78	6·77	7·06	6·71	5·85	7·03	6·51	6·23	6·25	6·36	6·56	6·21	5·95	6·31	5·84	5·44	5·64	6·10	7·35	5·14	4·88	5·24
CaO	10·50	7·18	10·88	6·89	9·11	9·83	10·97	8·94	8·79	8·23	11·34	9·51	9·64	10·09	8·90	9·55	10·83	7·58	10·69	10·68	10·18	9·23	9·89	7·81	9·84	7·86
Na_2O	2·58	3·02	1·50	1·97	3·31	2·45	2·62	2·94	2·22	3·06	2·16	2·42	2·28	2·45	2·44	2·20	2·58	3·56	2·16	2·39	2·39	2·15	2·55	3·03	2·49	2·86
K_2O	1·07	2·23	0·10	1·90	1·50	1·15	0·49	1·37	1·87	1·20	0·18	1·74	1·35	0·61	1·38	1·31	0·43	0·85	0·77	0·84	1·06	2·27	0·91	1·30	0·34	1·14
P_2O_5	0·27	0·15	0·14	0·14	0·19	0·23	0·13	0·17	0·15	0·16	0·25	0·23	0·19	0·23	0·22	0·21	0·23	0·24	0·22	0·26	0·25	0·24	0·19	0·21	0·29	0·22
LOI	1·77	2·66	5·55	3·31	2·62	n.d.	3·28	2·75	2·12	3·08	1·12	2·16	2·93	2·52	2·95	2·23	1·68	3·53	3·38	4·63	4·77	2·86	n.d.	2·29	2·79	2·45
mg-no.	0·56	0·60	0·73	0·68	0·62	0·58	0·61	0·59	0·55	0·61	0·54	0·59	0·56	0·56	0·58	0·57	0·54	0·55	0·54	0·54	0·52	0·56	0·58	0·47	0·41	0·45
Trace elements (ppm)																										
Sc	28	27	29	16	28	31	34	23	29	26	34	29	31	31	29	29	34	28	34	29	31	27	29	28	29	30
V	277	246	225	214	235	272	259	243	262	239	325	268	288	291	293	271	307	276	286	289	288	261	378	349	430	379
Cr	234	320	927	435	259	252	309	138	137	297	268	198	172	184	181	166	191	195	170	160	165	198	305	79	119	60
Ni	65	96	326	143	102	84	111	107	45	92	67	44	36	32	37	43	34	45	34	22	32	43	110	77	74	79
Zn	95	86	80	90	76	90	84	86	89	86	95	86	90	100	97	84	96	94	90	101	99	88	99	118	144	127
Cu	95	77	78	74	122	113	112	92	104	90	109	67	96	113	75	91	85	77	73	89	70	73	105	112	195	108
Rb	16·5	64·6	2·2	38·7	41·6	24·0	15·3	37·9	54·4	36·4	2·6	26·7	25·6	13·4	35·8	22·6	6·3	14·6	15·4	16·1	20·6	41·9	18·6	36·1	4·7	26·7
Sr	320	306	81	337	940	673	299	497	327	344	250	460	405	361	494	353	379	254	287	311	306	402	457	510	269	516
Y	29	24	20	21	18	24	19	22	27	23	28	25	25	26	25	24	28	26	25	30	25	26	24	35	50	35
Zr	137	109	78	98	113	122	80	105	135	108	153	132	126	133	134	120	131	135	127	165	142	132	139	155	191	168
Nb	8·05	5·93	4·11	6·59	5·15	6·64	4·19	6·19	5·51	5·29	5·10	6·42	6·02	6·40	6·24	5·12	6·03	5·85	5·26	7·07	6·04	5·75	6·73	6·81	7·48	6·55
Ba	508	780	29	762	509	986	79	533	531	387	173	821	1029	369	773	772	311	421	327	327	330	1463	174	295	157	334
La	20·43	13·94	15·13	15·34	13·82	17·22	9·43	15·73	13·89	13·98	9·16	12·52	10·62	12·34	11·93	9·96	12·05	12·26	10·67	14·20	12·35	12·33	14·91	17·28	17·82	15·56
Ce	41·76	27·72	34·76	27·94	27·41	34·42	18·81	30·33	28·67	27·22	20·56	26·46	23·01	26·09	25·40	21·62	26·39	26·30	22·81	31·18	26·62	26·24	34·56	36·38	40·47	33·53
Nd	22·18	14·49	22·83	13·25	14·57	18·04	10·46	15·02	16·90	14·64	14·45	16·43	14·28	16·21	15·87	13·79	16·35	16·18	14·94	18·76	16·41	16·14	21·52	20·64	26·93	19·85
Sm	5·05	4·11	7·25	3·66	3·76	4·72	3·17	4·06	4·79	4·16	4·38	4·72	4·28	4·82	4·59	4·05	4·62	4·69	4·42	5·20	4·81	4·52	5·16	6·12	8·32	5·92
Eu	1·79	1·28	2·52	1·22	1·31	1·57	1·11	1·31	1·52	1·33	1·83	1·67	1·62	1·71	1·65	1·51	1·73	1·64	1·53	1·75	1·66	1·66	1·88	2·09	2·90	2·07
Gd	5·64	4·34	8·18	3·82	3·68	4·65	3·45	4·12	5·39	4·54	5·14	5·18	4·64	4·92	4·83	4·65	5·17	5·22	4·87	5·80	5·29	5·11	5·49	6·66	9·74	6·64
Tb	0·91	0·78	1·52	0·68	0·63	0·79	0·63	0·71	0·94	0·78	0·87	0·85	0·83	0·86	0·84	0·80	0·89	0·86	0·83	0·97	0·98	0·87	0·89	1·21	1·71	1·22
Yb	2·24	1·98	3·29	1·71	1·55	1·96	1·67	1·93	2·41	2·01	2·25	2·18	2·07	2·21	2·12	1·90	2·26	2·16	2·16	2·44	2·19	2·18	1·87	2·59	3·67	2·68
Lu	0·34	0·31	0·47	0·26	0·23	0·30	0·25	0·29	0·36	0·31	0·33	0·33	0·32	0·33	0·33	0·29	0·34	0·33	0·33	0·37	0·33	0·33	0·26	0·37	0·53	0·39
Hf	3·53	2·75	2·00	2·38	2·26	2·81	1·97	2·66	3·79	2·79	3·80	3·37	3·30	3·52	3·34	3·13	3·50	3·56	3·36	4·27	3·65	3·48	3·83	4·16	5·46	4·07
Ta	0·44	0·35	0·24	0·37	0·25	0·32	0·24	0·34	0·36	0·35	0·26	0·35	0·33	0·36	0·34	0·32	0·35	0·37	0·34	0·42	0·37	0·36	0·44	0·43	0·49	0·41
Th	1·60	1·72	1·01	2·66	0·88	1·13	1·01	1·63	1·83	1·72	0·38	0·48	0·47	0·51	0·44	0·44	0·54	0·53	0·47	0·73	0·59	0·49	1·52	2·25	1·58	1·96
Pb	4·27	2·65	3·11	4·00	3·38	3·46	2·72	3·87	4·67	3·15	2·19	3·59	4·31	2·78	3·40	2·61	4·03	3·07	3·36	4·74	4·19	3·26	3·06	4·00	4·00	3·79
U	0·38	0·41	0·29	0·61	0·19	0·25	0·20	0·33	0·47	0·41	0·11	0·17	0·17	0·19	0·16	0·15	0·17	0·17	0·16	0·20	0·18	0·17	0·27	0·51	0·41	0·45

Table 1: continued

Sample:	P27-AVL	VF51 85	VF72-85	P24-AVL	P29-AVL	P31-AVL	VF24-85	VF34-85	VF50-85	VF63-85	UP203-AVL	UP205-AVL	UP209-AVL	UP212-AVL	SK214-AVL	SK215-AVL	SK216-AVL	SK219-AVL	VF110-85	VF111-85	VF145-85	VF146-85	VF152-85
Type:*	CT2	CT2	CT2	CT3	CT3	CT3	CT3	CT3	CT3	CT3	CT3	CT3	CT3	CT3	CT3	CT3	CT3	CT3	CT3	CT3	CT3	CT3	CT3
Location:	P	B	B	P	P	P	PR	PR	SR	B	UP	UP	UP	UP	SK	SK	SK	SK	S	S	KB	KB	KB
Major and minor elements (wt %)†																							
SiO_2	50·42	55·09	50·49	51·92	52·26	52·33	51·06	51·44	51·24	51·43	51·61	53·43	49·45	52·11	49·83	52·16	51·12	48·85	53·69	51·69	50·87	53·25	51·59
TiO_2	1·77	2·25	3·08	1·46	1·64	1·66	1·87	1·50	1·44	1·64	1·49	2·71	1·18	1·70	1·39	1·36	1·68	1·38	2·46	1·49	1·80	2·67	1·50
Al_2O_3	14·08	13·12	13·06	14·52	14·51	14·86	14·42	14·23	15·07	15·16	14·68	13·13	12·02	15·97	12·90	13·70	15·58	13·48	13·30	14·33	14·75	13·15	14·04
FeO_{tot}	10·60	12·49	14·77	11·01	11·23	11·06	12·06	10·95	11·39	11·34	10·19	12·91	11·67	10·58	11·30	10·17	11·04	10·66	13·03	10·79	11·40	13·57	11·58
MnO	0·18	0·17	0·17	0·18	0·18	0·18	0·18	0·19	0·18	0·19	0·17	0·22	0·18	0·16	0·18	0·18	0·18	0·18	0·20	0·19	0·20	0·24	0·19
MgO	7·98	4·68	5·29	7·17	6·91	6·18	6·18	7·20	6·47	6·82	7·53	4·63	13·47	5·36	12·86	9·09	6·13	13·36	4·41	7·02	6·69	4·56	7·46
CaO	12·34	8·08	9·61	10·00	8·44	10·09	11·02	11·36	11·52	9·90	12·06	9·96	9·83	10·87	9·86	10·74	10·50	10·05	9·76	11·76	10·75	8·47	10·68
Na_2O	2·16	2·86	2·39	2·21	2·78	2·41	2·63	2·47	2·30	2·60	1·97	2·27	1·57	2·59	1·21	1·76	2·61	1·70	2·32	2·28	2·59	2·36	2·07
K_2O	0·23	1·06	0·89	1·23	1·69	0·93	0·28	0·48	0·20	0·70	0·10	0·26	0·49	0·42	0·26	0·66	0·88	0·19	0·50	0·23	0·66	1·31	0·73
P_2O_5	0·15	0·20	0·26	0·18	0·25	0·21	0·30	0·20	0·19	0·21	0·18	0·47	0·13	0·25	0·20	0·19	0·28	0·14	0·34	0·22	0·30	0·41	0·17
LOI	2·23	1·92	3·00	2·04	2·10	n.d.	1·10	1·76	2·68	2·45	1·36	0·52	1·20	0·15	3·85	2·40	2·00	n.d.	1·59	1·62	2·35	2·12	1·88
mg-no.	0·61	0·44	0·43	0·58	0·56	0·54	0·52	0·58	0·54	0·56	0·61	0·43	0·71	0·52	0·70	0·65	0·54	0·72	0·42	0·58	0·55	0·41	0·57
Trace elements (ppm)																							
Sc	33	24	26	26	44	19	33	34	32	30	33	32	29	29	24	27	28	35	33	37	29	27	30
V	415	371	383	307	338	325	352	335	311	349	323	417	275	310	288	272	328	311	411	319	340	455	309
Cr	414	55	115	296	307	153	211	283	195	191	354	66	1117	226	744	426	258	1085	59	290	260	26	324
Ni	154	62	110	72	54	51	65	67	66	59	88	23	412	62	329	138	74	486	16	63	75	8	96
Zn	80	114	140	92	90	99	101	88	89	92	86	120	86	86	87	73	88	82	119	86	95	146	86
Cu	185	103	146	93	125	117	136	133	109	126	107	157	87	39	86	82	117	108	160	125	125	152	97
Rb	2·4	26·6	19·8	29·4	39·6	17·3	4·9	8·2	2·5	16·8	0·7	2·7	7·0	3·9	2·6	9·1	16·2	2·9	6·3	3·1	10·4	22·3	9·3
Sr	226	474	373	361	525	301	304	325	278	451	215	261	218	353	184	242	317	199	259	290	260	245	272
Y	22	30	43	25	25	27	25	23	21	25	22	41	17	22	19	20	24	17	36	23	25	36	23
Zr	86	140	173	93	109	100	96	78	77	90	75	184	64	100	69	72	100	56	142	86	94	147	88
Nb	3·13	6·20	6·74	3·97	3·94	4·21	4·50	2·92	2·86	3·46	3·26	11·43	3·36	4·35	3·64	3·45	4·68	2·18	6·61	4·08	4·57	7·41	3·40
Ba	70	207	239	601	1169	424	235	218	93	398	104	284	176	201	104	360	404	112	371	240	351	787	309
La	4·97	14·49	14·94	8·11	7·69	7·62	8·49	5·45	5·17	6·43	5·86	17·50	5·26	6·83	6·78	6·38	8·65	3·59	13·16	7·63	8·38	13·81	6·87
Ce	12·22	30·93	33·83	17·95	17·49	17·07	19·27	12·56	12·19	14·70	13·28	37·72	11·77	15·78	15·13	14·13	18·98	8·53	29·06	16·99	19·27	30·17	15·45
Nd	10·53	17·37	22·83	12·07	12·45	12·02	13·56	9·79	9·30	10·91	9·85	24·06	8·47	11·90	10·27	9·78	13·08	6·90	19·48	11·69	13·47	19·79	10·91
Sm	3·85	5·26	7·30	3·85	3·95	4·01	4·25	3·42	3·27	3·79	3·28	6·98	2·82	3·84	3·19	3·18	3·97	2·38	6·16	3·82	4·41	6·33	3·60
Eu	1·43	1·90	2·52	1·37	1·47	1·53	1·58	1·36	1·32	1·49	1·30	2·41	1·06	1·55	1·22	1·21	1·53	1·04	2·21	1·44	1·65	2·19	1·36
Gd	4·34	6·34	8·66	4·35	4·58	4·72	5·23	4·32	4·14	4·66	4·07	7·73	3·38	4·42	3·86	3·71	4·77	3·04	7·35	4·47	4·97	7·31	4·32
Tb	0·79	1·06	1·50	0·80	0·83	0·87	0·85	0·76	0·72	0·83	0·71	1·32	0·58	0·73	0·67	0·66	0·82	0·54	1·25	0·77	0·86	1·26	0·76
Yb	1·73	2·55	3·30	2·10	2·08	2·24	2·11	1·96	1·90	2·12	1·82	3·33	1·58	1·81	1·64	1·64	2·07	1·37	3·18	1·92	2·12	3·20	2·03
Lu	0·26	0·37	0·47	0·32	0·33	0·33	0·32	0·30	0·29	0·32	0·26	0·48	0·22	0·26	0·24	0·24	0·30	0·20	0·48	0·29	0·32	0·49	0·30
Hf	2·46	3·73	5·13	2·31	2·55	2·64	2·55	2·07	1·98	2·31	2·00	4·97	1·71	2·56	1·92	1·84	2·55	1·44	4·08	2·19	2·62	4·29	2·31
Ta	0·17	0·44	0·48	0·21	0·22	0·22	0·29	0·19	0·18	0·21	0·19	0·63	0·20	0·27	0·20	0·20	0·26	0·13	0·39	0·23	0·28	0·46	0·20
Th	0·23	1·92	1·53	0·52	0·28	0·36	0·37	0·24	0·22	0·36	0·25	0·94	0·17	0·26	0·29	0·27	0·42	0·11	0·78	0·40	0·32	1·00	0·28
Pb	0·98	3·85	3·46	2·57	2·19	2·25	2·22	1·21	1·26	1·47	1·26	3·74	1·54	1·84	1·17	1·63	2·24	0·71	3·23	1·60	2·38	3·60	1·55
U	0·06	0·49	0·73	0·13	0·10	0·11	0·10	0·08	0·07	0·11	0·07	0·23	0·04	0·09	0·08	0·08	0·11	0·03	0·24	0·11	0·10	0·29	0·10

Table 1: continued

Sample:	VF88-85	VF89-85	VF91-85	VF126-85	VF129-85
Type:*	CT3	CT3	CT3	CT3	CT3
Location:	PD	PD	PD	M	M
Major and minor elements (wt %)†					
SiO_2	50·89	53·32	50·86	49·51	49·00
TiO_2	1·43	2·19	1·17	1·50	1·97
Al_2O_3	14·89	14·01	14·34	15·14	14·46
FeO_{tot}	10·31	13·31	10·75	10·72	12·44
MnO	0·18	0·20	0·19	0·17	0·17
MgO	8·09	4·22	7·40	7·92	6·21
CaO	11·34	9·60	12·99	12·57	12·46
Na_2O	2·02	2·37	2·00	2·12	2·27
K_2O	0·62	0·47	0·18	0·17	0·77
P_2O_5	0·18	0·32	0·12	0·19	0·26
LOI	2·22	1·67	1·46	2·29	1·53
mg-no.	0·62	0·40	0·59	0·61	0·51
Trace elements (ppm)					
Sc	30	32	31	34	31
V	301	378	290	295	391
Cr	408	67	284	546	407
Ni	141	19	65	170	108
Zn	86	113	81	78	87
Cu	56	156	142	95	129
Rb	7·8	5·8	2·5	1·0	4·6
Sr	282	296	225	317	341
Y	24	33	19	17	25
Zr	76	136	64	80	104
Nb	3·23	5·97	2·48	4·93	6·76
Ba	249	289	149	140	377
La	6·49	11·92	4·77	5·70	8·28
Ce	14·94	26·31	10·40	13·79	19·46
Nd	10·26	17·68	7·87	10·18	14·44
Sm	3·03	5·56	2·83	3·20	4·63
Eu	1·31	1·95	1·14	1·31	1·78
Gd	4·09	6·60	3·59	3·86	5·35
Tb	0·71	1·10	0·63	0·63	0·86
Yb	1·90	2·95	1·62	1·40	1·86
Lu	0·29	0·44	0·24	0·20	0·29
Hf	2·12	3·71	1·73	2·02	2·76
Ta	0·19	0·35	0·15	0·38	0·53
Th	0·25	0·72	0·30	0·21	0·31
Pb	1·12	3·57	1·03	0·93	0·90
U	0·07	0·21	0·08	0·06	0·08

n.d., not determined; LOI, loss on ignition; *mg*-number = Mg/(Mg + 0·85Fe), atomic.
*CT1–CT3 refer to geochemically different basalt types recognized in Vestfjella (see text). Abbreviations for sample locations: B, Basen; P, Plogen; PR, Pukkelryggen; SR, Salryggen; S, Skansen; PD, Pagodromen; KB, Kjakebeinet; SK, Steinkjeften; M, Muren; UP, Utpostane.
†The compositions are normalized to 100% volatile free.

Plagioclase is by far the most abundant phenocryst phase and typically occurs as glomerocrysts. Augite occurs as separate euhedral phenocrysts, subhedral granular aggregates, or glomerocrysts with plagioclase and olivine. Orthopyroxene phenocrysts have been identified in few lava flows only. Unaltered olivine is rare in the lavas, but many samples contain pseudomorphs after euhedral or slightly resorbed olivine phenocrysts. Chromian spinel inclusions are present in augite, orthopyroxene and olivine phenocrysts. The groundmass is aphanitic or fine grained, typically intersertal and consists of plagioclase laths, subhedral augite ± pigeonite, quenched Fe–Ti oxides, minor sulphides and cryptocrystalline mesostasis.

Most of the Vestfjella lavas are altered. Olivine and orthopyroxene are commonly replaced by green or brown phyllosilicates and plagioclase is variably sericitized or saussuritized. In the most altered units, fresh plagioclase is rare and clinopyroxene is partially replaced by chlorite. The samples from Utpostane (Fig. 1) record low-grade metamorphism, most probably as a result of intrusion of the Utpostane gabbro; in many specimens, augite is replaced by tremolite–actinolite.

The bulk of the exposed strata consist of compound lava flows that show the characteristic features of inflated pahoehoe flows (Self *et al.*, 1996) with pipe amygdules at the bases and highly amygdaloidal upper parts. The lava units range from thin flow lobes to sheet flows exceeding 20 m in thickness. The samples for this study were collected from the massive interiors of the flow units to avoid amygdules. Nevertheless, many of the analysed samples contain small (<1 mm) dictytaxitic voids filled with secondary minerals, mainly chlorite. In the Utpostane suite, the predominant void-filling minerals are chlorite and tremolite–actinolite.

GEOCHEMISTRY

Major and trace elements

Chemical compositions of Vestfjella CFBs are listed in Table 1 and the Appendix. The data exhibit notably variable SiO_2 (47·9–56·5 wt %), TiO_2 (0·88–3·53 wt %), K_2O (0·02–2·39 wt %), P_2O_5 (0·11–0·47 wt %) and *mg*-number [atomic ratio of $Mg/(Mg + 0{\cdot}85Fe_{tot})$] (0·74–0·40) (Fig. 2; Table 1). The rocks are subalkaline and range from basalt to basaltic andesite. On the basis of the CIPW norms (Yoder & Tilley, 1962) they may be classified as olivine and quartz tholeiites.

The major and trace elements exhibit compositional trends typical of tholeiites with, for example, negative correlation of FeO_{tot} and TiO_2 with *mg*-number. Al_2O_3 first increases with decreasing *mg*-number and then decreases when *mg*-number is <0·55 (Fig. 2). Trace elements with high ionic potential, such as Ni and Zr, typically show considerable ranges (Ni from 486 to 8 ppm; Zr

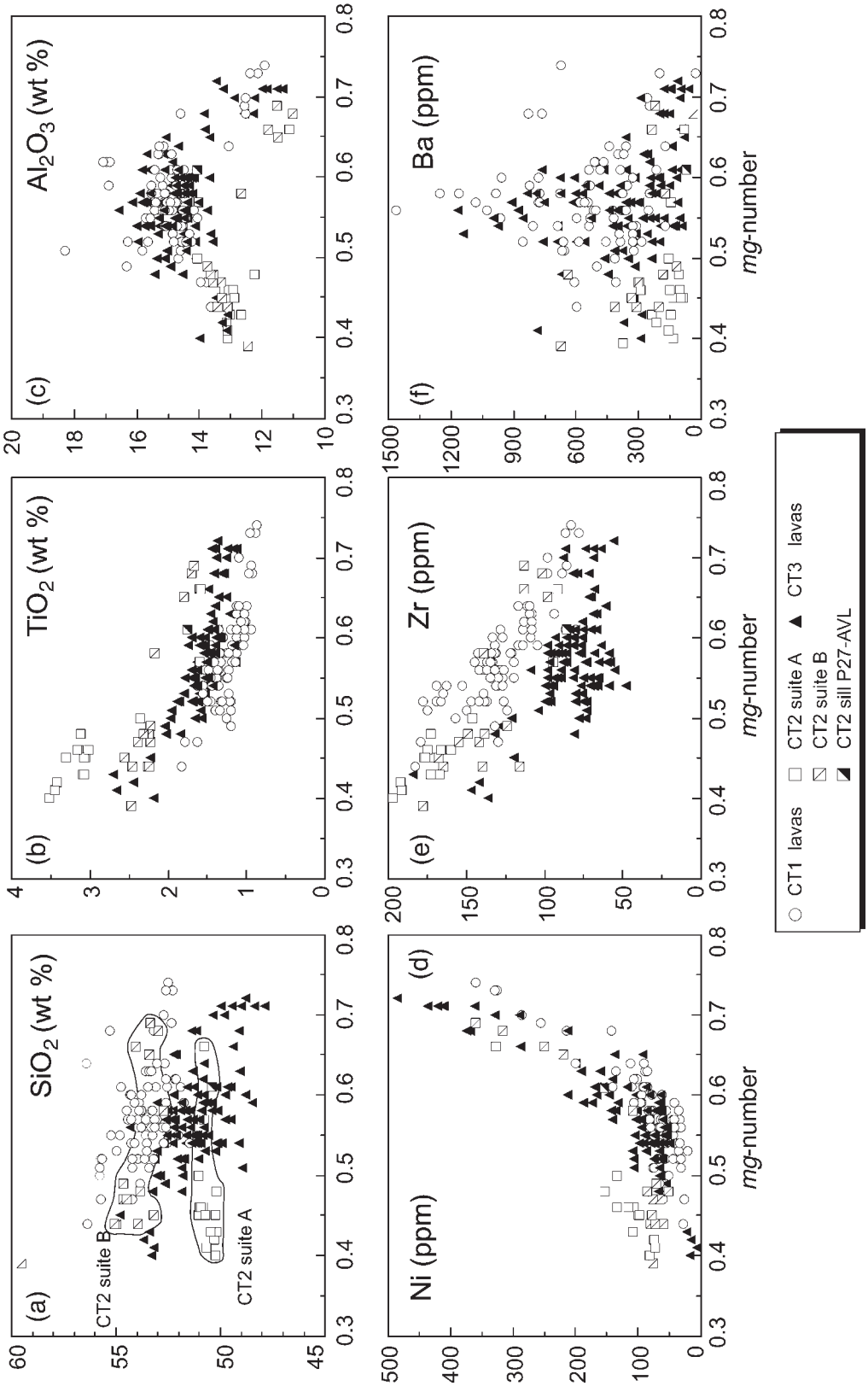

Fig. 2. Variations in (a) SiO_2, (b) TiO_2, (c) Al_2O_3, (d) Ni, (e) Zr and (f) Ba vs *mg*-number in CT1, CT2 and CT3 of Vestfjella. CT2 lava suites A and B and the sill sample P27-AVL are depicted.

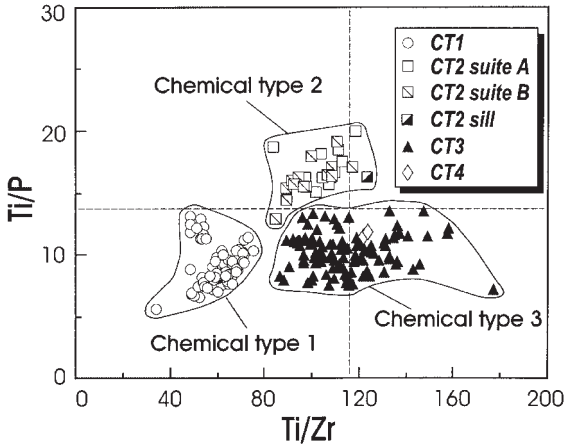

Fig. 3. Variations in Ti/Zr vs Ti/P in Vestfjella CFBs. Primitive mantle values (Sun & McDonough, 1989) are shown by stippled lines. Data for CT4 dyke rocks are from Luttinen *et al.* (1998).

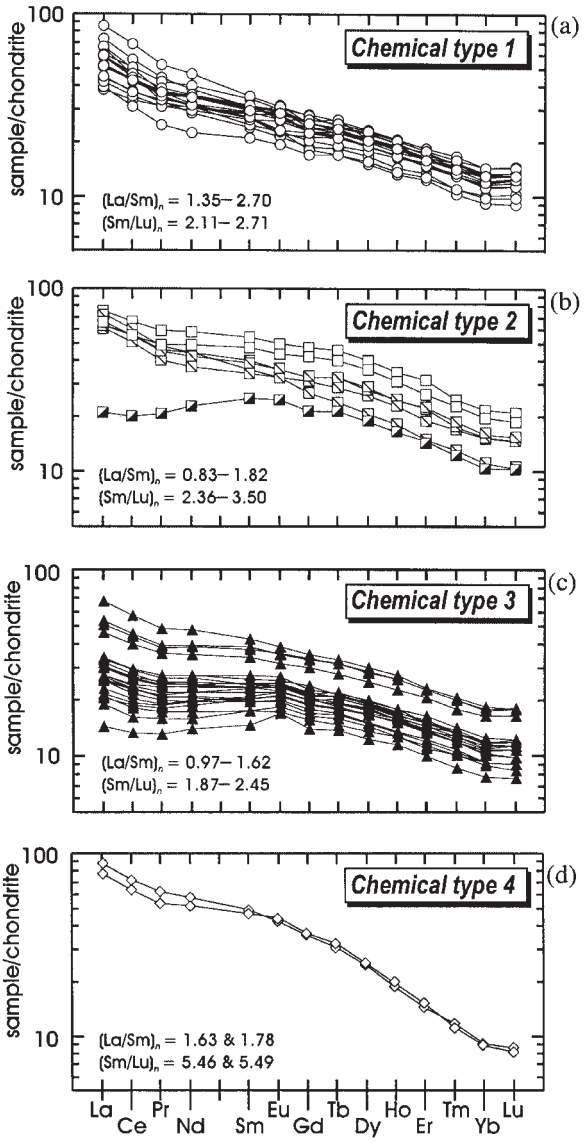

Fig. 4. Chondrite-normalized REE diagrams for (a) CT1, (b) CT2, (c) CT3 and (d) CT4 of Vestfjella. Normalizing values after Sun & McDonough (1989). Symbols for CT2 subtypes as in Fig. 2. Data for CT4 are from Luttinen *et al.* (1998).

from 48 to 238 ppm) and good correlations with *mg*-number, whereas alkali and alkaline earth metals in general show large scatter and poor correlation with *mg*-number (Fig. 2).

An important feature of the Vestfjella CFBs is that they fall naturally into three subgroups based on incompatible high field strength element (HFSE) and REE ratios. Such ratios are not considered to be susceptible to subsolidus alteration, fractional crystallization or small variations in degree of melting of peridotitic mantle sources. Basalts with notably different ratios thus represent different magmatic lineages with different evolution or mantle sources, or both. The plot of Ti/Zr vs Ti/P (Fig. 3) shows grouping for the new analyses demonstrating that the previously proposed subdivision for the CFBs of Basen and Plogen (Luttinen & Siivola, 1997) is applicable throughout Vestfjella. Following the nomenclature of Luttinen & Siivola (1997) the groups have been designated chemical types 1, 2 and 3 (CT1, CT2 and CT3) (Fig. 3). The CT4 dyke rocks of Luttinen *et al.* (1998) have Ti/Zr and Ti/P similar to those of CT3 (Fig. 3) but otherwise have a different overall geochemical composition.

The most diagnostic features of CT1, CT2, CT3 and CT4 can be summarized as follows. CT1 exhibits low Ti/Zr (<80) and TiO_2 compared with CT2 and CT3. It is also characterized by relatively high SiO_2 and $(La/Sm)_n$ and low Ni (Figs 2–4). CT2 shows considerable within-group variations. All CT2 rocks have near primitive mantle Ti/Zr and are characterized by high FeO_{tot}, TiO_2 and Ti/P, and low Al_2O_3 in comparison with CT1 and CT3 (Figs 2 and 3). The $(La/Sm)_n$ values typically are lower than those of CT1 (Fig. 4). A sill rock sample P27-AVL exhibits the most light REE (LREE)-depleted pattern among the Vestfjella CFBs with $(La/Sm)_n$ of 0·83. A unique feature of CT2 is the bimodal distribution of SiO_2 contents leading to recognition of CT2 suites A and B (Fig. 2). The CT3 lavas exhibit near primitive mantle Ti/Zr and Ti/P and low HFSE (such as Zr) (Fig. 2) and REE concentrations relative to CT1 and CT2. Their REE patterns resemble those of CT2 with relatively low $(La/Sm)_n$. In comparison, the CT4 dykes are notably rich in TiO_2, Zr and other HFSE regarding their relatively high *mg*-number of 0·64 (Luttinen *et al.*, 1998) and show strong enrichment in LREE with $(La/Lu)_n$ of 8·9 and 9·8 (Fig. 4).

The incompatible element signatures of the Vestfjella CFB types are illustrated in mantle-normalized diagrams in Fig. 5. CT1, CT2 and CT3 typically exhibit negative Nb and Ta anomalies and positive Ba, K and Sr anomalies but have otherwise different patterns. All CT1 rocks show relative enrichment of LREE, positive Ba and K anomalies, and a distinctive negative Ti anomaly; this is designated the common signature of CT1. Most of the CT1 lavas further record a positive Sr anomaly and a negative P anomaly (Fig. 5). A subgroup of CT1 lavas, however, is distinguished by relatively high $(P/Nd)_n$ and low $(Th/Ta)_n$ (Fig. 5). The CT2 rocks typically exhibit enrichment from HREE to Rb. The sill rock P27-AVL, however, shows affinity to depleted MORB in terms of $(La/Nd)_n$, $(Th/Ta)_n$ and $(Rb/Th)_n$ <1 but exhibits positive Ba, K and Sr anomalies. The CT2 tholeiites do not record a negative Ti anomaly but the lavas exhibit a distinctive negative P anomaly. The incompatible element signature of CT3 is rather similar to that of the low $(Th/Ta)_n$ subgroup of CT1 in terms of low Th and U and the pronounced positive Ba, K and Sr anomalies (Fig. 5). The CT3 rocks lack the negative Ti anomaly of CT1 and are less enriched in LREE. Besides Ba, K and Sr their pattern is relatively smooth and akin to that of MORB. The CT4 dykes have smooth patterns with an affinity to ocean island basalts (OIBs) (Fig. 5; Luttinen *et al.*, 1998).

In summary, the four basaltic rock types of Vestfjella exhibit many differences in their chemical composition. The most abundant types, CT1 and CT3, have high Al_2O_3 and low FeO_{tot} and TiO_2 compared with CT2, show pronounced positive Ba and K anomalies in mantle-normalized diagrams, and also exhibit a broad negative correlation between SiO_2 and *mg*-number (Figs 2–5).

Geochemical stratigraphy

Stratigraphic variations in Ti/Zr, Ti/Y and *mg*-number for >200 lava samples from Vestfjella are illustrated in Fig. 6. CT1 is readily distinguished from CT2 and CT3 on the basis of Ti/Zr apart from a few intermediate cases. TiO_2 content and Ti/P have been used to divide the data into the CT2 and CT3 magma types (see Luttinen & Siivola, 1997).

The key features of the geochemical stratigraphy include: (1) preponderance of CT1 in the northern area (Basen, Plogen, Dagvola, Dagvolinga, Grushallet, Pukkelryggen and Salryggen) and CT3 in the southern area (Skansen, Pagodromen, Muren, Kjakebeinet, E and W Steinkjeften, and Utpostane); (2) repeated alternation of the three magma types (most notably in Basen and Plogen); (3) abundance of CT2 close to the base of the Basen and Plogen sections; (4) different Ti/Y of the lower and upper CT1 lavas in the Plogen section. Otherwise, the geochemical stratigraphy shows little evidence of systematic variations and, similar to many CFB suites, the basalt types show rather uniform compositions with intermediate *mg*-number values from the bottom to the top (cf. Arndt *et al.*, 1998).

The CT1 lavas may be subdivided into a lower and an upper suite based on their Ti/Y values. Throughout Vestfjella, the CT1 lavas that crop out over 600 m above sea level exhibit relatively high Ti/Y ratios (typically >300) (Fig. 6). These lavas are underlain by a succession of CT3-dominated flows in many localities. In the south, the few CT1 flows below the 600 m level at E and W Steinkjeften and Utpostane exhibit high Ti/Y ratios. At Pagodromen, however, the lower CT1 flows record low Ti/Y similar to those of the lower CT1 lavas in the north. It is possible that the CT3–CT1 transition within 600–800 m above sea level represents a regional stratigraphic horizon. If this is correct, then the predominance of CT3 in the southern area may, at least partially, be an artefact of exposure, and the CT3 suite could have erupted on low-Ti/Y CT1 throughout Vestfjella (Fig. 6).

Vestfjella region is characterized by major faulting structures and many sections show evidence of post-volcanic vertical movements (Furnes *et al.*, 1987; Luttinen & Siivola, 1997). It is difficult to estimate the magnitude of fault-related displacements over the large distances between the sampled sections. To reconstruct the regional lava stratigraphy, the sections in Fig. 6 are arranged so that the CT3–CT1 transition coincides vertically. This requires fairly small height adjustments within the two major outcrop areas in the north (Basen, Plogen, Dagvola, Dagvolinga, Grushallet, Pukkelryggen and Salryggen) and south (Skansen, Pagodromen, Muren, Kjakebeinet, E and W Steinkjeften, and Utpostane) (Fig. 1). The sections in the south, however, have been generally moved up ~100 m relative to the sections in the north. The two sections at Steinkjeften have been elevated more, up to ~200 m (W Steinkjeften). The correlation between W Steinkjeften and Kjakebeinet is based on CT2 interbeds. Considering the distance of ~120 km between Utpostane and Basen (Fig. 1), the deviations from the present positions are rather small in the reconstruction and may be explained by the regional W–SW dip and the post-volcanic faulting. The reconstruction in Fig. 6 shows the Vestfjella CFB suite to consist of three major stratigraphic units: the lower suite of CT1-dominated flows (Ti/Y <300), the middle suite of CT3-dominated flows and the upper suite of CT1-dominated flows (Ti/Y >300). The CT2 suite A and B lavas (Fig. 2) are confined to levels below and above 200 m, respectively (Fig. 6).

Published data on 34 dyke and sill rocks that cut the lava sequence expand this discussion to later magmatic stages. On the basis of Ti/Zr and Ti/P ratios and TiO_2

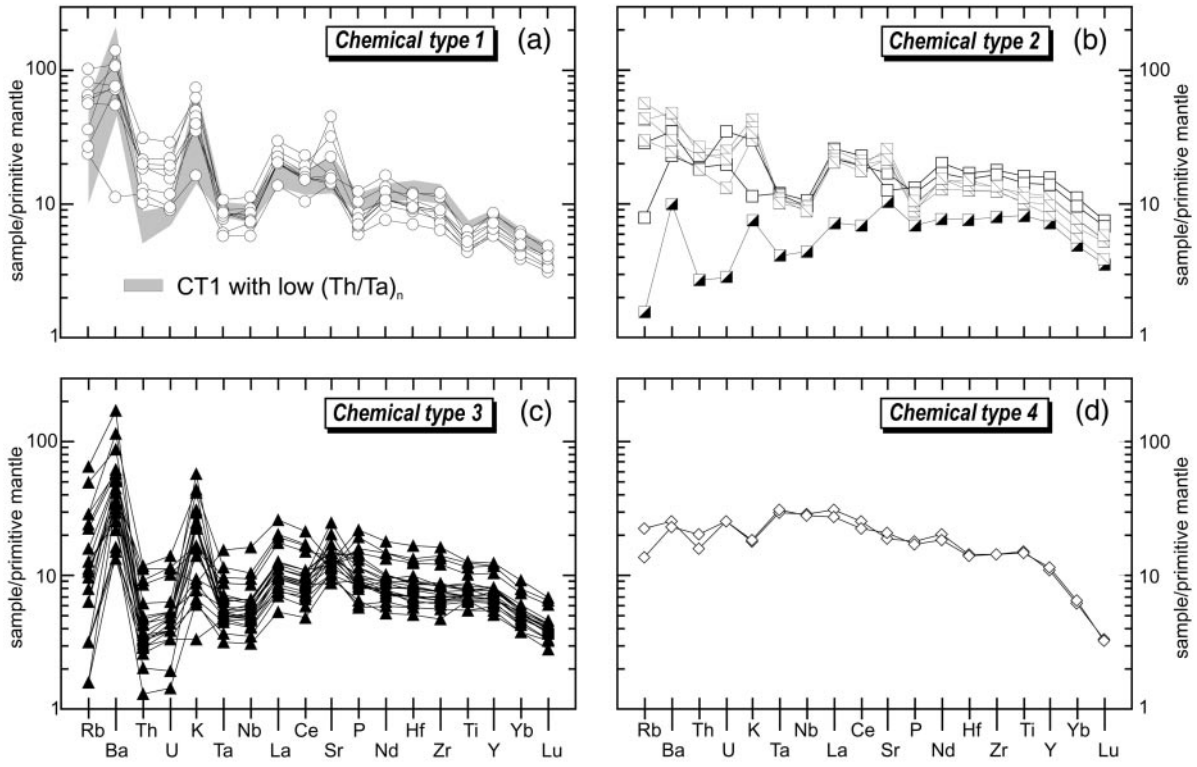

Fig. 5. Primitive mantle-normalized incompatible element diagrams for (a) CT1, (b) CT2, (c) CT3 and (d) CT4 of Vestfjella. The grey pattern in (a) includes nine CT1 lavas with low $(Th/Ta)_n$ relative to those of other CT1 lavas. Symbols for CT2 subtypes as in Fig. 2. Normalizing values after Sun & McDonough (1989). Data for CT4 are from Luttinen *et al.* (1998).

contents at given *mg*-number, it is possible to recognize four distinct dyke populations that show affinities to CT1, CT2, CT3 and CT4. Data of Furnes and Mitchell (1978) suggest that the dykes of south Vestfjella (Muren, Kjakebeinet, E and W Steinkjeften, Pagodromen and Skansen) belong almost exclusively to CT3 and only one out of 24 dykes shows affinity to CT1. In contrast to the volcanic record, CT2 is more abundant than CT1 among the studied dyke and sill rocks of north Vestfjella, with five out of 10 analysed samples featuring a CT2 affinity (Luttinen *et al.*, 1998; this study). CT3 dykes have not been reported from the north. Two of the studied dykes record an OIB-like CT4 signature (Luttinen *et al.*, 1998) suggesting this magma type occurs only as a minor dyke phase and is confined to north Vestfjella. In summary, the dyke rock data imply an increase in CT2 magmatism and a decrease in CT1 and CT3 magmatism associated with the later magmatic stages in the north Vestfjella. CT3 seems to have dominated magmatism in the south Vestfjella area throughout the volcanic episode recorded by the exposed part of the CFB succession. Emplacement of CT4 magmas was confined to relatively late magmatic stages in north Vestfjella.

Nd and Sr isotopes

New neodymium and strontium isotope data on 26 lavas and a sill rock from Vestfjella are listed in Table 2. The CT1 samples record highly variable Nd isotopic compositions. The ε_{Nd} (at 180 Ma) values range from $-2{\cdot}5$ to $-15{\cdot}9$ and show a bimodal distribution with a gap between a group with ε_{Nd} from $-2{\cdot}5$ to $-4{\cdot}1$ and two samples with ε_{Nd} of $-11{\cdot}1$ and $-15{\cdot}9$ (henceforth referred to as the high-ε_{Nd} and low-ε_{Nd} types, respectively) (Fig. 7). The CT2 samples also exhibit a wide range of ε_{Nd} values ($+7{\cdot}6$ to $-7{\cdot}5$). The ε_{Nd} of CT3 cluster around chondritic values ($+2{\cdot}0$ to $-2{\cdot}2$), with the majority being slightly positive.

The high-ε_{Nd} and low-ε_{Nd} CT1 lavas are characterized by different initial ε_{Sr} values: those with distinctly low ε_{Nd} exhibit ε_{Sr} (180 Ma) of $+33{\cdot}4$ and $+64{\cdot}7$, whereas the others cluster between $+8{\cdot}6$ and $+20{\cdot}7$. The CT2 lavas record a wide range of ε_{Sr} values from $-15{\cdot}7$ to $+49{\cdot}6$. The CT3 lavas show narrower range than CT1 and CT2 and have ε_{Sr} from $-11{\cdot}0$ to $+5{\cdot}5$.

Generalizing, the new isotopic results from eight sections throughout the Vestfjella range accord with the previously published values (Luttinen *et al.*, 1998) for

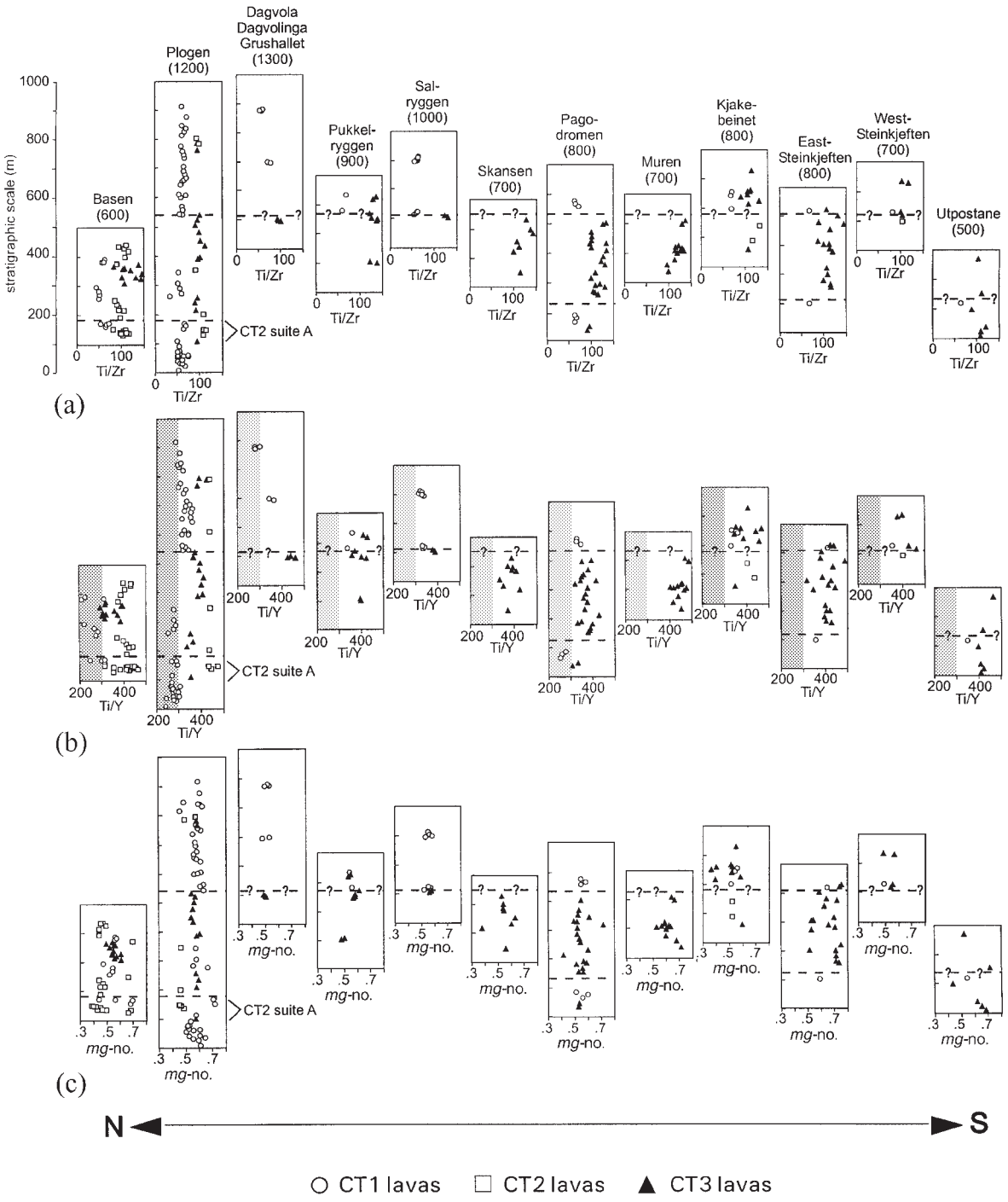

Fig. 6. Variations in (a) Ti/Zr, (b) Ti/Y and (c) *mg*-number of Vestfjella lavas in 12 sections. Section localities are indicated in Fig. 1. The upper dashed line indicates a potential correlation horizon based on a widespread CT3–CT1 transition. Question marks indicate sections with dubious CT3–CT1 transition. The lower dashed line shows a possible correlation horizon related to CT1–CT3 transition and the grey area in (b) points to Ti/Y values <300, which characterize the lower CT1 suite. The CT2 suite A is indicated below the lower dashed line. Numbers below the section names indicate the height of the top of the section in metres above sea level. Data sources: Furnes & Mitchell (1978); Furnes *et al.* (1987); Luttinen *et al.* (1998); this work.

Table 2: Isotopic data of Mesozoic flood basalts in Vestfjella, Dronning Maud Land, Antarctica

Sample	Location*	Sm† (ppm)	Nd† (ppm)	$^{147}Sm/^{144}Nd$	$^{143}Nd/^{144}Nd$‡	ε_{Nd}§	Rb† (ppm)	Sr† (ppm)	$^{87}Rb/^{86}Sr$	$^{87}Sr/^{86}Sr$‡	ε_{Sr}§
Chemical type CT1											
VF-57-85	Basen	5·05	22·18	0·1377	0·512000 ± 4	−11·1	16·5	320	0·1470	0·707029 ± 22	+33·4
VF-80-85	Plogen	4·16	14·64	0·1718	0·511795 ± 6	−15·9	36·4	344	0·3016	0·709623 ± 11	+64·7
VF-26-85	Pukkelryggen	4·62	16·35	0·1708	0·512476 ± 6	−2·6	6·3	379	0·0474	0·705019 ± 8	+8·6
VF-30-85	Pukkelryggen	4·69	16·18	0·1752	0·512460 ± 6	−3·0	14·6	254	0·1638	0·705330 ± 11	+8·8
VF-40-85	Salryggen	4·42	14·94	0·1789	0·512492 ± 4	−2·5	15·4	287	0·1529	0·705858 ± 30	+16·7
VF-44-85	Salryggen	5·20	18·76	0·1676	0·512450 ± 4	−3·0	16·1	311	0·1475	0·706123 ± 26	+20·7
VF-46-85	Salryggen	4·81	16·41	0·1772	0·512466 ± 4	−2·9	20·6	306	0·1919	0·706104 ± 26	+18·8
VF-147-85	Kjakebeinet	4·05	13·79	0·1776	0·512408 ± 8	−4·1	22·6	353	0·1825	0·705466 ± 14	+10·1
VF-81-85	Pagodromen	4·52	16·14	0·1693	0·512441 ± 9	−3·3	41·9	402	0·2971	0·705805 ± 28	+10·7
Chemical type CT2											
VF-51-85	Basen	5·26	17·37	0·1831	0·512240 ± 4	−7·5	26·6	474	0·1599	0·708197 ± 11	+49·6
VF-72-85	Basen	7·30	22·83	0·1933	0·512522 ± 7	−2·2	19·8	373	0·1513	0·706573 ± 13	+26·9
P55-AVL¶	Plogen	5·16	21·52	0·1450	0·512569 ± 10	−0·2	18·6	457	0·1160	0·705820 ± 14	+17·5
P27-AVL¶	Plogen	3·57	11·25	0·1919	0·513024 ± 5	+7·6	2·4	226	0·0303	0·703262 ± 13	−15·7
Chemical type CT3											
VF-63-85	Basen	3·79	10·91	0·2100	0·512709 ± 5	+1·0	16·8	451	0·1062	0·704737 ± 1	+2·5
VF-24-85	Pukkelryggen	4·25	13·56	0·1895	0·512622 ± 4	−0·2	4·9	304	0·0459	0·704705 ± 46	+4·2
VF-34-85	Pukkelryggen	3·42	9·79	0·2112	0·512744 ± 7	+1·7	8·2	325	0·0719	0·704036 ± 12	−6·2
VF-50-85	Salryggen	3·27	9·30	0·2126	0·512743 ± 7	+1·6	2·5	278	0·0256	0·703872 ± 11	−6·9
VF-110-85	Skansen	6·16	19·48	0·1921	0·512602 ± 7	−0·6	6·3	259	0·0693	0·704090 ± 12	−5·4
VF-111-85	Skansen	3·82	11·69	0·1976	0·512528 ± 7	−2·2	3·1	290	0·0305	0·704406 ± 8	+0·5
VF-88-85	Pagodromen	3·03	10·26	0·1785	0·512693 ± 8	+1·5	7·8	282	0·0788	0·703720 ± 22	−11·0
VF-89-85	Pagodromen	5·56	17·68	0·1901	0·512624 ± 4	−0·2	5·8	296	0·0558	0·704061 ± 18	−5·3
VF-91-85	Pagodromen	2·83	7·87	0·2174	0·512718 ± 7	+1·0	2·5	225	0·0317	0·704254 ± 12	−1·7
VF-145-85	Kjakebeinet	4·41	13·47	0·1979	0·512579 ± 6	−1·2	10·4	260	0·1140	0·704567 ± 32	−0·2
VF-146-85	Kjakebeinet	6·33	19·79	0·1934	0·512571 ± 8	−1·3	22·3	245	0·2594	0·705342 ± 9	+5·5
VF-152-85	Kjakebeinet	3·60	10·91	0·1995	0·512677 ± 6	+0·7	9·3	272	0·0974	0·703971 ± 15	−8·1
VF-126-85	Muren	3·20	10·18	0·1900	0·512733 ± 6	+2·0	1·0	317	0·0090	0·703658 ± 14	−9·3
VF-129-85	Muren	4·63	14·44	0·1938	0·512648 ± 40	+0·2	4·6	341	0·0384	0·703679 ± 18	−10·1

*See Fig. 1.
†Analysed with ICP-MS at the Washington State University apart from samples P55-AVL and P27-AVL (see below).
‡$^{143}Nd/^{144}Nd$ normalized to $^{146}Nd/^{144}Nd = 0·7219$, $^{87}Sr/^{86}Sr$ to $^{86}Sr/^{84}Sr = 0·1194$. Within-run error expressed as $2\delta_m$ in the last significant digits.
§Initial ε_{Nd} and ε_{Sr} values, calculated at 180 Ma using $^{143}Nd/^{144}Nd = 0·51264$ and $^{147}Sm/^{144}Nd = 0·1966$, and $^{87}Sr/^{86}Sr = 0·7045$ and $^{87}Rb/^{86}Sr = 0·0816$, respectively.
¶Sm, Nd, Rb, and Sr concentrations and isotopic ratios analysed at the Geological Survey of Finland [for analytical methods, see Luttinen *et al.* (1998)].

eight lavas and four dykes from the Basen and Plogen sections. The available data show a broad negative correlation between initial ε_{Nd} and ε_{Sr} values (Fig. 7). The CT1 rocks plot in two groups along a low-ε_{Nd}–high-ε_{Sr} continuation of the oceanic mantle array (see Menzies & Murthy, 1980). The high-ε_{Nd} group of CT1 comprises the group with low $(Th/Ta)_n$ (Fig. 5) delineating a previously unknown subtype of CT1. The CT2 dykes and sill plot within the depleted part of the mantle array as do most of the CT3 lavas and the CT4 dyke. The CT2 lavas, on the other hand, plot in two groups aside from the mantle array as a result of relatively high ε_{Sr} at given ε_{Nd}. The two CT2 lavas with the lowest ε_{Nd} belong to the high-SiO_2 suite B (Fig. 2), whereas those with near-chondritic ε_{Nd} have low SiO_2 and belong to suite A apart from sample P55-AVL. The ε_{Nd} value of the CT2

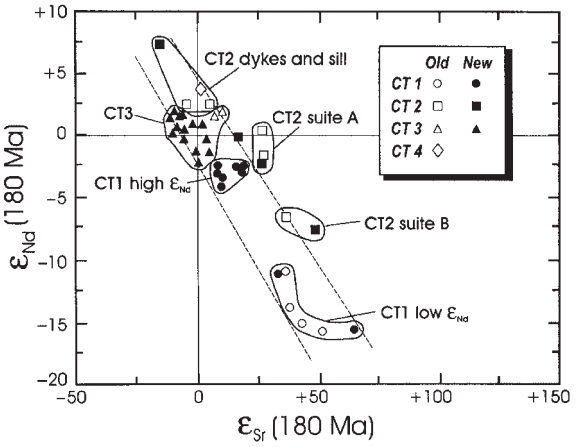

Fig. 7. Initial Sr and Nd isotopic compositions of Vestfjella CFBs presented in ε_{Sr} vs ε_{Nd} diagram. Previously published analyses (Luttinen *et al.*, 1998) are are shown for comparison. The dashed lines feature the oceanic mantle array and its low-ε_{Nd}–high-ε_{Sr} continuation (see Menzies & Murthy, 1980).

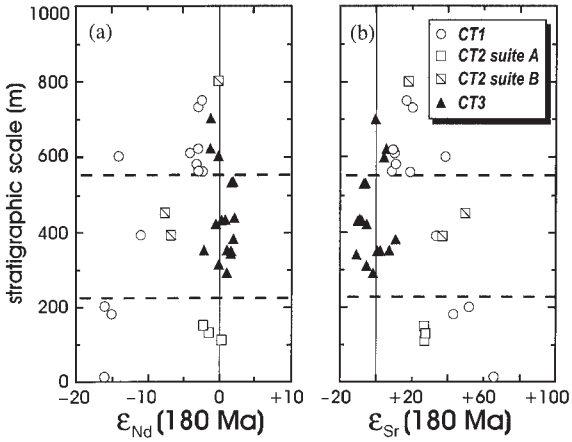

Fig. 8. Stratigraphic variations in ε_{Nd} (180 Ma) and ε_{Sr} (180 Ma) of Vestfjella lavas assuming reconstruction of Fig. 6. The dashed lines at ~550 m and 220 m indicate divisions between the upper, middle and lower suites. Data sources: Luttinen *et al.* (1998); this work.

sill rock sample P27-AVL (+7·6) is the highest so far reported for Karoo CFBs in Africa and Antarctica, and approaches the isotopic composition of depleted mantle at 180 Ma (DePaolo, 1981*a*).

Isotopic stratigraphy

Isotopic data of Vestfjella CFBs are combined in Fig. 8, where ε_{Nd} and ε_{Sr} are plotted using the proposed stratigraphic reconstruction (Fig. 6). The figure demonstrates dominance of CT1 with low ε_{Nd} and high ε_{Sr} at low elevations and CT1 with high ε_{Nd} and low ε_{Sr} at high elevations. It should be noted, however, that CT1 lavas with high and low $(Th/Ta)_n$ values (Fig. 5) are interbedded in the upper part of the Plogen section. Judging from this and the fact that all the high-ε_{Nd} CT1 lavas exhibit low $(Th/Ta)_n$, it is probable that low-ε_{Nd} lavas also occur above the 600 m level.

The CT2 samples close to the base of the succession show near-chondritic ε_{Nd} and ε_{Sr} (Fig. 8) and belong to the CT2 suite A (Figs 2 and 6). The overlying set of CT2 flows record distinctly negative ε_{Nd} and positive ε_{Sr} and belong to the CT2 suite B. The single CT2 flow at 800 m level (P55-AVL) has a near-chondritic ε_{Nd} value and a slightly positive ε_{Sr} (Fig. 8) different from the other suite B rocks. The CT3 lavas show a relatively uniform isotopic composition throughout the lava pile. The overall isotopic stratigraphy and the positive ε_{Nd} of the cross-cutting CT2 dykes and the sill rock (P27-AVL) and the CT4 dyke (Fig. 7) suggest a general increase in ε_{Nd} values during the Vestfjella CFB magmatism.

Alteration effects

The scatter of major and trace element data (Fig. 2) probably reflects the net result of variable melt compositions, phenocryst abundances and subsolidus alteration. Detailed assessment of alteration effects is beyond the scope of this study. We deal here with the effects of alteration on incompatible elements and isotopic ratios. Studies on altered basalts have demonstrated that elements with low ion potential, such as Rb, K, Ba and Sr, are often mobile whereas HFSE and REE retain their abundances fairly well (e.g. Wood *et al.*, 1976).

Alteration effects on incompatible trace elements

A geochemical traverse through a CT3 lava flow of 16 m thickness (Appendix) illustrates compositional differences between the amygdaloidal, strongly altered lava crust and the massive flow core (Fig. 9). High LOI values reflect abundant secondary phyllosilicates in voids and alteration products of magmatic minerals in the lava crust. Concentrations of Ni, Nb, Zr and Y are nearly constant from the base to the top of the flow, demonstrating within-flow homogeneity and immobility of HFSE. In the flow core, Rb, Ba and Sr contents show relatively small variations (4–7, 199–273 and 258–269 ppm, respectively). In the upper crust, Rb and Ba are clearly lower ($\leq$2 and $\leq$30 ppm, respectively) and Sr contents generally higher (up to 442 ppm) than in the core. The variation of K is similar to that of Rb. Variations of the trace element contents within the core of lava flows are further illustrated by three analyses from an extensive CT2 lava flow of 10 m thickness (Appendix), which show wide ranges of Rb (1–22 ppm), K_2O (0·22–1·12 wt %) and Ba (137–217 ppm), and a narrow range of Sr (264–295 ppm) in comparison with relatively

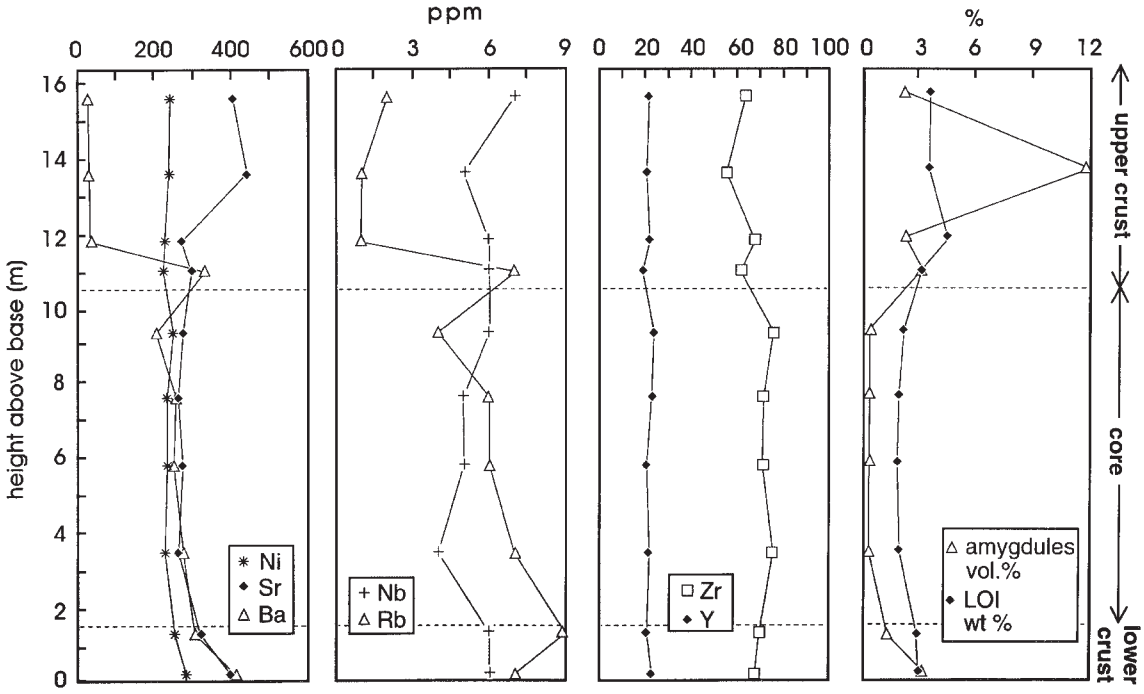

Fig. 9. Variations of selected trace elements, LOI and the content of amygdules in a CT3 lava flow from Skansen, south Vestfjella.

constant Zr (191–197 ppm). These examples lead to the following (qualitative) conclusions: (1) the relative mobility seems to have been Rb ≈ K > Ba ≫ Sr; (2) alteration has decreased concentrations of Rb, K and Ba rather than increased them.

The behaviour of mobile elements is of special interest in the case of CT3 lavas, which, with the exception of high LILE, exhibit incompatible element patterns akin to those of depleted MORB (Fig. 5). It is essential to determine whether the selective enrichment of Ba, K and Sr results from alteration or reflects original magmatic compositions. The examples presented above imply that strong enrichment of LILE is an unlikely result of alteration (see Harris *et al.*, 1990). Assuming that the LILE concentrations have been significantly modified by secondary processes, we would expect some of the rocks to show depletion of Ba relative to other highly incompatible elements. In contrast, the CT3 samples representing a stratigraphic section of >600 m thickness show similar incompatible element signatures with $(Ba/Nb)_n$ consistently higher than two (Fig. 5). The identical REE patterns of the metamorphosed CT3 lavas from the Utpostane section (Fig. 1; Table 1) and the unmetamorphosed CT3 lavas form other sections in Fig. 4 lend support to immobility of REE.

We conclude that although concentrations of Rb, K, Ba and Sr of individual samples should be viewed with caution it is unlikely that the high overall LILE contents are solely an alteration effect. They more probably represent a regional feature related to the magmatic evolution of the Vestfjella CFBs. It is possible that, on average, the whole-rock analyses of flow cores approximate magmatic compositions of CT1, CT2 and CT3 also in the case of LILE.

Alteration effects on Nd and Sr isotopes

Recent studies on Ferrar tholeiites have demonstrated pronounced changes in the Sr isotopic signatures even in rocks that appear relatively unaltered (Fleming *et al.*, 1995). On the other hand, Nd isotopic systematics in extensively altered rocks may still reflect magmatic compositions (Landoll *et al.*, 1994; Foland *et al.*, 1997). It is important to evaluate possible effects of subsolidus alteration on the Sr isotopic compositions of the Vestfjella CFBs.

Whereas CT1, CT3 and the intrusive CT2 define a broad linear array ($r^2 = 0{\cdot}87$) in the ε_{Nd} vs ε_{Sr} diagram, the CT2 lavas are distinct owing to high ε_{Sr} at given ε_{Nd} (Fig. 7). It is rather unlikely that the samples that plot within the 'mantle array' have been significantly affected with regard to their Sr isotopic compositions. The high ε_{Sr} values of the CT2 lavas, on the other hand, are a typical feature of many hydrothermally altered basic rocks (Fleming *et al.*, 1995; Foland *et al.*, 1997).

It is probable that the degree of alteration has been largely controlled by the access of hydrothermal fluids

to the lava flows (see Bevins *et al.*, 1991). The CT2 lavas are no different from CT1 and CT3 in terms of vesicularity and jointing or LOI values and petrographic evidence of degree of alteration. Similar to CT1 and CT3, they further record low $^{87}Rb/^{86}Sr$ (Table 2). The measured $^{87}Sr/^{86}Sr$ ratios thus closely correspond to the Sr isotopic compositions immediately after the closure of the system with regard to Rb and Sr, presumably in the Jurassic. If the Sr isotopic ratios of the CT2 lavas have been significantly increased as a result of subsolidus alteration, a specific, Sr isotopically different fluid is required that circulated in the sporadic CT2 interbeds but avoided the intercalated CT1 and CT3 flows. Such an explanation seems unlikely and further could not explain why the samples with high ε_{Sr} values also have different immobile incompatible element characteristics from the rocks with lower ε_{Sr} values: negative correlation between ε_{Nd} and Th/Ta (Fig. 10a) suggests the latter has not been affected by alteration. Accordingly, the positive correlation between ε_{Sr} and Th/Ta (Fig. 10b) and the fact that only the high-ε_{Sr} rocks exhibit a marked negative P anomaly (Fig. 5) indicate that the high ε_{Sr} values of the CT2 lavas reflect magmatic compositions.

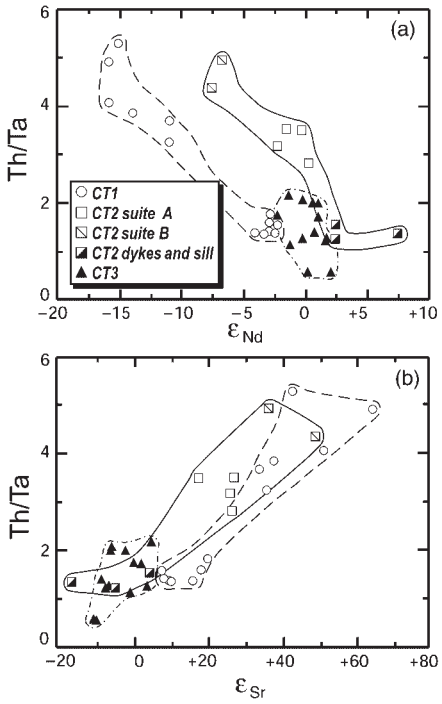

Fig. 10. Variations of (a) ε_{Nd} and (b) ε_{Sr} vs Th/Ta in Vestfjella CFBs. Data sources: Luttinen *et al.* (1998); this work.

Cause of regional alteration

Pronounced subsolidus alteration of lavas is a regional feature of Vestfjella. By comparison, the basalts in Kirwanveggen and Heimefrontfjella are relatively unaltered. One possible explanation for this difference is the abundance of crosscutting intrusive equivalents of CFBs in Vestfjella.

The replacement of augite by amphibole in the Utpostane basalts is a likely consequence of contact metamorphism as a result of the emplacement of the Utpostane gabbro. Geophysical surveys have indicated sources of magnetic anomalies beneath the Högisen ice dome, N–NW of the Muren gabbro and beneath the Plogbreen ice stream between Basen and Plogen (Fig. 1); these have been interpreted as Jurassic intrusions (Corner, 1994; Ruotoistenmäki & Lehtimäki, 1997). It is thus possible that gabbroic intrusions of variable size characterize the entire Vestfjella region. Furthermore, the CFBs are cut by abundant dolerite dykes and less abundant sills. Emplacement of the various intrusive rock types could have promoted hydrothermal circulation of fluids and the alteration of the lavas.

Relationships to other Karoo CFBs

It has been generally accepted that western Dronning Maud Land was juxtaposed to southeast Africa before break-up of Gondwana, although the details of Jurassic configuration remain an issue of discussion (e.g. du Toit, 1937; Martin & Hartnady, 1986; Lawver & Scotese, 1987). The reconstruction of Martin & Hartnady (1986) has been widely used and it places western Dronning Maud Land adjacent to the Lebombo Monocline of Africa (Fig. 1). Accordingly, the Mesozoic CFBs of these areas have been reported to show isotopic and geochemical similarities (Faure *et al.*, 1979; Harris *et al.*, 1990, 1991; Luttinen & Siivola, 1997; Luttinen *et al.*, 1998).

Cox (1992) has proposed a tight Jurassic fit of southeast Africa and East Antarctica, which positions the Vestfjella and south Lebombo areas notably close to each other. We have taken this to be the initial configuration and examine here the incompatible element and Nd and Sr isotopic signatures of the CFB rock types of the Lebombo and western Dronning Maud Land to evaluate possible relationships between them. In Vestfjella, the main magma types can be recognized based on Ti/Zr and Ti/P alone (Fig. 3). More informative, for a regional comparison of Karoo CFBs in Africa and Antarctica, are depleted MORB-normalized incompatible element patterns and specifically the diagnostic Nb, P and Ti anomalies shown by the various rock types. For the comparison, we have divided the various Karoo CFBs into low-Ti, high-Ti and transitional types (see Cox *et al.*, 1967; Erlank *et al.*, 1988).

Low-Ti rock types

Low-Ti tholeiites dominate the CFB successions of Vestfjella, Kirwanveggen and southern to central Lebombo Monocline (Erlank, 1984; Harris *et al.*, 1990; Sweeney *et al.*, 1994). All of the low-Ti basalts exhibit a pronounced negative Nb anomaly (Fig. 11). Geochemical and Nd and Sr isotopic similarities led Luttinen & Siivola (1997) and Luttinen *et al.* (1998) to propose that the low-ε_{Nd} CT1 suite of Vestfjella represents a counterpart of the low-ε_{Nd} type of Sabie River basalts of southernmost Lebombo. Few REE analyses have been reported for the Sabie River basalts in this area (Erlank, 1984). Nevertheless, averages of the two magma types show high Ba_n and nearly indistinguishable trace element patterns from La to Yb with low $(P/Nd)_n$ (0·56 and 0·69) and $(Ti/Gd)_n$ (0·71 and 0·75) and high $(La/Yb)_n$ (9·35 and 9·76) (Fig. 11). Both rock types further exhibit lower $(Nb/La)_n$ (0·17 and 0·42) and ε_{Nd} (180 Ma) values (< -10) and higher ε_{Sr} (180 Ma) values ($> +25$) than the other low-Ti basalts (Figs 11 and 12). The average Nb_n value (1·1) of the representative southern Lebombo basalts is notably lower than that of the low-ε_{Nd} CT1 basalts (2·8). It should be noted, however, that data for 34 Sabie River basalts, southern Lebombo (Erlank, 1984) show Nb_n of 0·9–6·8 with an average of 2·2, which is rather similar to the average value for the low-ε_{Nd} CT1.

Our new data for the high-ε_{Nd} CT1 type and CT3 bring detail to the correlation between the low-Ti CFBs in Africa and Antarctica. Relative to the low-ε_{Nd} CT1 and Sabie River basalts of south Lebombo the other low-Ti rocks show slightly higher $(Nb/La)_n$ (0·49–0·61), $(P/Nd)_n$ (0·69–1·16), $(Ti/Gd)_n$ (0·85–1·09) and ε_{Nd} (> -6), and lower $(La/Yb)_n$ (3·92–7·15) and ε_{Sr} ($< +25$) (Figs 11 and 12). Overall, these rock types show many similarities but clear correlatives are not apparent. The high-ε_{Nd} subtype of CT1 exhibits similar isotopic compositions to those of some Sabie River basalts of the central Lebombo (Fig. 12), but the latter have higher TiO_2 and lower SiO_2 at the same *mg*-number (Sweeney *et al.*, 1994) as well as relatively higher $(Rb/Ba)_n$ and $(Th/K)_n$ (Fig. 11). In terms of Sr isotopic compositions the high-ε_{Nd} CT1 also shows affinity to Kirwan basalts (Fig. 12). Furthermore, both types record a small negative P anomaly and rather similar patterns from K to Yb in general. The Kirwan basalts have notably lower Ba_n contents and higher ε_{Nd} values, however (Figs 11 and 12).

Similarities between the CT3 lavas and the Kirwan basalts include relatively high $(Ti/Gd)_n$ (1·03 and 0·97) and low $(La/Yb)_n$ (4·64 and 3·92) and near-chondritic ε_{Nd} ($+3$ to -3) (Figs 11 and 12). The high Ba_n and low ε_{Sr} of CT3 stand in contrast to the lower Ba_n and higher ε_{Sr} of Kirwan basalts. Harris *et al.* (1990) have pointed out chemical similarities between the Kirwan basalts and the Sabie River basalts of south Lebombo. Judging from the Nd isotopic compositions and relatively low $(Ba/Nb)_n$, the Kirwan basalts resemble the extrusive equivalents of the Rooi Rand dykes rather than the low-Ti Sabie River basalts of southern Lebombo (Fig. 12).

Transitional rock types

Similar to Rooi Rand dolerites and their extrusive equivalents (e.g. Hawkesworth *et al.*, 1984; Duncan *et al.*, 1990), CT2 shows affinity to high-Ti flood basalt types based on high Ti/Y (mostly from 300 to 600) but their Zr/Y are typically low (<6) and within the range of low-Ti CFBs (Erlank *et al.*, 1988). Compared with the low-Ti and high-Ti rock types, these rock types have intermediate TiO_2 at given *mg*-number. Hence, they can be regarded as transitional types between low-Ti and high-Ti CFBs.

Both transitional rock types are spatially associated with low-Ti basalts and occur as crosscutting dykes and interbedded lavas. Luttinen & Siivola (1997) and Luttinen *et al.* (1998) have previously pointed out geochemical and Nd and Sr isotopic similarities between the CT2 and Rooi Rand magma types. These are characterized by variable incompatible element patterns and, for this reason, representative CT2 and Rooi Rand dykes are compared with the average of the CT2 lavas in Fig. 11. Some rocks exhibit a strong MORB affinity with rather low LREE relative to heavy REE (HREE), MORB-like HFSE ratios and positive initial ε_{Nd} (up to $+8$). Others, such as the CT2 lavas, record LREE enrichment, marked negative Nb and P anomalies and negative ε_{Nd} (Figs 11 and 12). Our new data on CT2 demonstrate similarity between the intrusive CT2 and the Rooi Rand magma type on one hand and difference between these rock types and the extrusive CT2 on the other. These differences imply that the CT2 lavas may correspond to contaminated differentiates of MORB-like CT2 parental magmas.

High-Ti rock types

Rocks belonging to the high-Ti category are abundant in Mwenezi area and the northern half of the Lebombo Monocline and characterize the Ahlmannryggen dyke swarm of Dronning Maud Land (e.g. Erlank *et al.*, 1988; Harris *et al.*, 1991; Sweeney *et al.*, 1994) (Fig. 1). In Vestfjella, the CT4 dykes show affinities to the high-Ti group based on notably high HFSE and LREE contents as well as Ti/Y (>400) and Zr/Y (5·7) at *mg*-number of 0·64.

We have subdivided the high-Ti rock types on the basis of $(Nb/La)_n$ and $(P/Nd)_n$ values (Fig. 11). The group with relatively high $(Nb/La)_n$ (0·69–1·13) and $(P/Nd)_n$ (0·66–0·91) includes the CT4 dykes, the high-Fe subtype of high-Ti rocks, central Lebombo (Sweeney *et al.*, 1994), and some of the Ahlmannryggen dykes (Harris *et al.*,

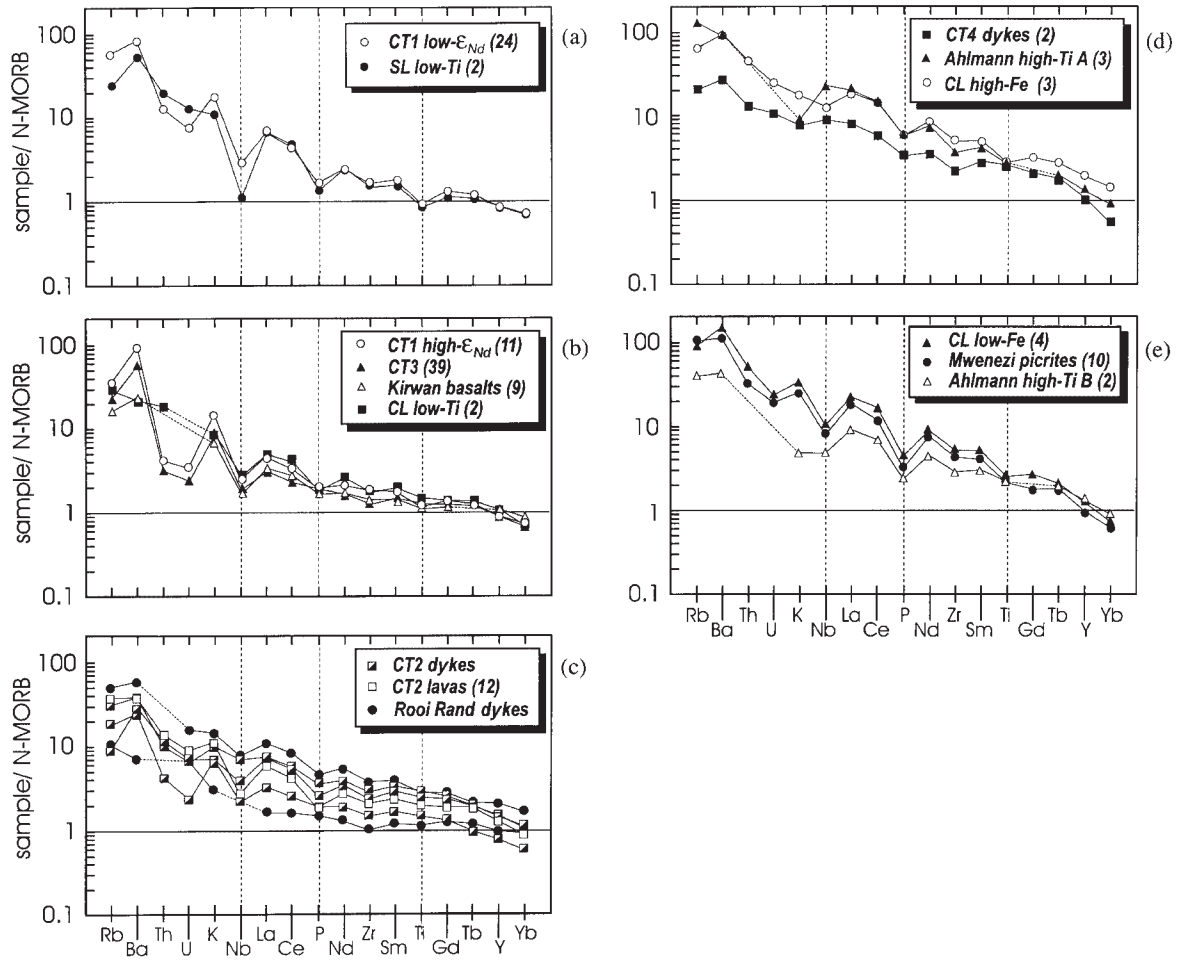

Fig. 11. N-MORB-normalized incompatible element patterns of Jurassic CFBs from southern Africa and Dronning Maud Land, Antarctica. SL low-Ti and CL low-Ti in (a) and (b) are averages of Sabie River low-Ti basalts from south Lebombo and central Lebombo, respectively. CL high-Fe and CL low-Fe in (d) and (e) are Sabie River high-Ti subtypes from central Lebombo. Ahlmann high-Ti A and B in (d) and (e) indicate two subtypes of high-Ti dykes from Ahlmannryggen. Normalizing values after Sun & McDonough (1989). Data sources: Erlank (1984); Harris *et al.* (1990, 1991); Ellam & Cox (1991); Sweeney *et al.* (1994); Luttinen *et al.* (1998); this work.

1991). These rocks have rather similar and smooth patterns with high $(La/Yb)_n$ (13·13–23·40) (Fig. 11). The CT4 dykes and the Ahlmannryggen dykes are in fact among the few rocks in the Karoo CFB province that do not exhibit a negative Nb anomaly (see Fig. 11). Some of the high-Fe rocks from central Lebombo resemble CT4 also in terms of Nd and Sr isotopic compositions (Fig. 12). Nd isotopic data have not been published for the Ahlmannryggen dykes but their ε_{Sr} (180 Ma) (−4 to +37; Harris *et al.*, 1991) extend to values that are comparable with those of the CT4 dykes and the high-Fe rocks of central Lebombo. The incompatible element pattern of the low-Fe subtype of the high-Ti rocks of central Lebombo (Sweeney *et al.*, 1994) is nearly identical with that of the Mwenezi picrites: both have distinctive negative Nb and P anomalies (shared also by some Ahlmannryggen dykes) and comparable ranges of ε_{Sr}, and their ε_{Nd} values extend to notably low values (Figs 11 and 12).

Summary of possible relationships

Judging from the Nd and Sr isotope data and the MORB-normalized incompatible element diagrams, unequivocal correlatives for Vestfjella magma types are not found among the low-Ti CFBs of the Lebombo Monocline and Kirwanveggen. The low-ε_{Nd} CT1 and the Sabie River basalts of southern Lebombo, however, exhibit many similarities and differ from the other low-Ti types. Another feature that links the southern Lebombo and northern Vestfjella is the similarity between the CT2 and Rooi Rand magma types. The high-ε_{Nd} CT1 and CT3 lavas,

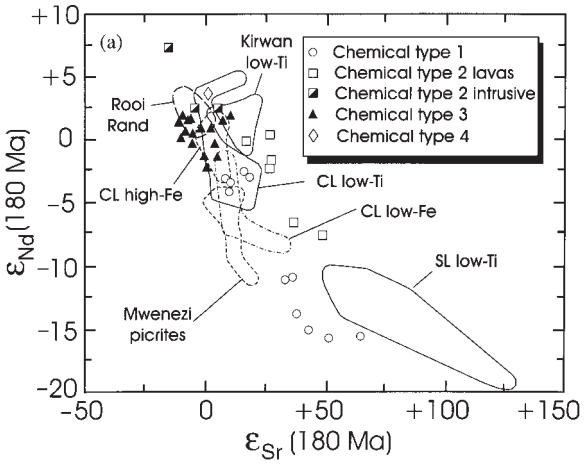

Fig. 12. ε_{Nd} (180 Ma) and ε_{Sr} (180 Ma) of Jurassic CFBs from southeast Africa and western Dronning Maud Land. Abbreviations as in Fig. 11. Data sources: Hawkesworth *et al.* (1984); Harris *et al.* (1990, 1991); Ellam & Cox (1991); Sweeney *et al.* (1994); Luttinen *et al.* (1998); this work.

which dominate in the southern part of Vestfjella, have notably high Ba contents and do not have obvious counterparts elsewhere in the Karoo volcanic province. The Kirwan basalts show intermediate features between the high-ε_{Nd} CT1 and the CT3 basalts with respect to HFSE and REE. In summary, the low-Ti succession of Vestfjella may correspond to a southward extension of the laterally heterogeneous Sabie River Basalt Formation of the Lebombo Monocline (see Duncan *et al.*, 1984; Hawkesworth *et al.*, 1984; Sweeney *et al.*, 1994).

The CT4 dykes show similarities to some high-Ti CFBs of Ahlmannryggen and central Lebombo. The other high-Ti rocks are characterized by spiked patterns with negative Nb and P anomalies resembling those of low-Ti and transitional CFBs (Fig. 11). More geochronological, geochemical and isotopic data are required for the Ahlmannryggen and CT4 dykes to address the genetic relationships between the high-Ti CFB types in detail.

DISCUSSION

In the following discussion emphasis will be placed on immobile incompatible trace elements and the Nd and Sr isotopic systematics. First we examine the compositional variations within each magma type and their implications of low-pressure differentiation. After that we will evaluate the petrogenetic relationships between the rock types and possible parental magma compositions and address processes that could have led to generation of the magma series. The importance of depleted and enriched mantle sources, magmatic plumbing systems, lithospheric terrane boundary and lithospheric thinning zones are also discussed and, eventually, a tectono-magmatic model for the Vestfjella CFBs is presented.

Low-pressure differentiation of the magma types

The CT1, CT2 and CT3 suites record wide geochemical ranges indicating effective magmatic differentiation. First we discuss the processes responsible for the variations observed in the volumetrically predominant magma types CT1 and CT3. Differentiation of the CT2 tholeiites is examined separately. The high-ε_{Nd} subtype of CT1 shows narrow compositional ranges and its liquid line of descent is thus poorly constrained. Therefore we focus our treatment here on the low-ε_{Nd} type. The high-*mg*-number CT4 dykes have nearly identical compositions (Luttinen *et al.*, 1998) and are excluded from the following section.

Fractional crystallization of CT1 and CT3

The phenocryst assemblages and geochemical variations suggest that early olivine-controlled fractionation and subsequent gabbroic fractionation, when *mg*-number was <0·55, were largely responsible for differentiation of the CT1 and CT3 suites. Least-squares mixing modelling (Morris, 1984) is hampered by the large scatter in major oxides, specifically SiO_2 at given *mg*-number (Fig. 3). Calculations with several parent–daughter pairs yield feasible results using fractionates consisting of olivine, augite and plagioclase, but the relative proportions of the minerals vary substantially (listings of least-squares models are available from the first author on request). Variations in isotopic and incompatible trace element ratios, however, are not highly susceptible to the exact composition of the fractionating assemblage. A fractionation sequence of olivine (70%) + augite (30%), when *mg*-number is >0·55, and olivine (20%) + plagioclase (50%) + augite (30%), when *mg*-number is <0·55, accords with the overall major oxide variations of the Vestfjella magma types. Olivine and plagioclase fractionation has little influence on most of the incompatible element ratios. Hence, the bulk D values for isotopic and trace element modelling are largely dependent on the augite abundance, which is 30% in both of the model fractionates.

Differentiation of CT1 and CT3 is modelled in Fig. 13a. The results demonstrate that the decrease of Sm/Nd in CT1 and CT3 cannot be explained by gabbroic fractionation (FC; Fig. 13a) alone and requires some sort of an open magmatic system, such as simultaneous assimilation of crust and fractionation (AFC; DePaolo, 1981*b*). An AFC process could potentially also account for the increase in SiO_2 as recorded by CT1 and CT3 (Fig.

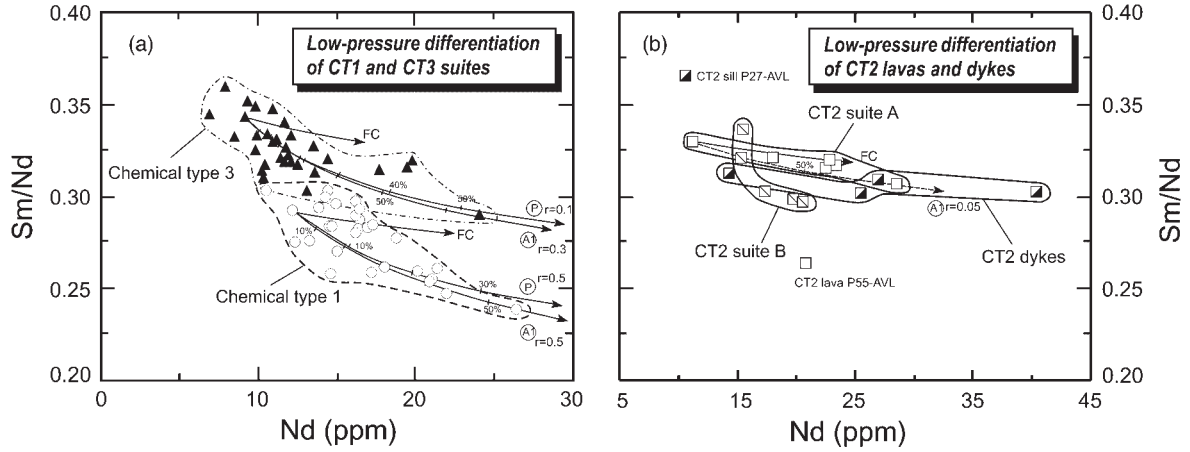

Fig. 13. Modelling of REE variations as a result of low-pressure differentiation of (a) CT1 and CT3 and (b) CT2 magma types. The arrow (FC) indicates 50% fractionation of olivine (20%), clinopyroxene (30%) and plagioclase (50%) with bulk D values for Nd and Sm of 0·12 and 0·18, respectively. AFC models with the same fractionate but different crustal contaminants and r values are indicated. Tick marks show 10% intervals of degree of fractionation. Mixing endmembers for CT1, CT2 and CT3 are P57-AVL, B16-AVL and B403-AVL, respectively. Contaminant A1 is xenolith X4-AVL and P is hypothetical Proterozoic crustal contaminant (Table 4). Data sources: Luttinen *et al.* (1998); this work.

2). We shall next consider possible crustal contaminants of the Vestfjella CFB magmas.

Possible crustal contaminants

Little is known about the basement that the Vestfjella CFBs intruded. In southern Vestfjella, however, some lavas and dyke rocks contain felsic crust-derived fragments. Two petrographically similar granitoid xenoliths record ε_{Nd} (180 Ma) values of −52 and −53, T_{DM} model ages (DePaolo, 1981*a*) of 3·27 and 3·24 Ga, and ε_{Sr} (180 Ma) values of +64 and +59 (Table 3). Geochemically, they resemble the 3·27 Ga (Farrow *et al.*, 1990) Anhalt Granitoid Suite trondhjemites of the Kaapvaal craton (Fig. 1) (see Hunter *et al.*, 1992) with relatively high SiO_2 and Na_2O/K_2O, and low FeO, MgO, TiO_2, Nb, Zr and Y relative to the average upper-crustal composition of Rudnick & Fountain (1995) (Table 4). Similar to Archaean tonalitic–trondhjemitic–granodioritic rocks, the HREE concentrations of these xenoliths are notably low (see Martin, 1987). An arkosic sandstone xenolith has ε_{Nd} (180 Ma) of −9, ε_{Sr} (180 Ma) of +155, a T_{DM} model age of 1·55 Ga, and plots along the ∼1 Ga errorchron defined by Maud Belt (Fig. 1) granitoids and gneisses from Heimefrontfjella [ε_{Nd} (180 Ma) −2 to −11; Arndt *et al.*, 1991]. The ε_{Sr} value is also comparable with the median ε_{Sr} (180 Ma) of +132 reported for felsic Maud Belt rocks (Moyes *et al.*, 1993). On the basis of these isotopic similarities the sandstone had probably a dominantly Proterozoic provenance and correlates with the Palaeozoic sedimentary sequence that is exposed at Fossilryggen and Vestfjella, and underlies the CFBs in northern Heimefrontfjella and Kirwanveggen (Fig. 1).

The granitoid xenoliths indicate that at least some of the Vestfjella magmas were emplaced through the Grunehogna craton (Fig. 1) and were contaminated with Archaean crustal material. We point out that the existence of Archaean xenoliths in southern Vestfjella does not necessarily indicate that the craton extends beneath this area. Flood basalt magmas have been recently shown to propagate considerable distances from their source regions on the surface as inflated pahoehoe flows (Self *et al.*, 1996) and also within the crust as dykes (LeCheminant & Heaman, 1989; Elliot *et al.*, 1999). We conclude that the Proterozoic basement as well as the Palaeozoic sedimentary rocks represent other plausible contaminants for the basalts.

AFC modelling of CT1 and CT3

The role of AFC in the magmatic evolution of the CT1 and CT3 suites is examined in Fig. 13a, which shows that incorporation of crustal material could account for the decrease in Sm/Nd. Modelling with an Archaean trondhjemitic contaminant (A1) as well as a hypothetical Proterozoic contaminant (P), yields feasible results suggesting a higher rate of assimilation in the case of CT1 (r = 0·5) than CT3 (r = 0·1 and 0·3). For the Archaean and Proterozoic contaminants we have used the geochemical data on xenolith X4-AVL and the average upper crust of Rudnick & Fountain (1995) (Table 4).

In the case of CT3 basalts, the decrease of ε_{Nd} along with *mg*-number lends support to operation of an AFC process (Fig. 14a). Models with an Archaean contaminant (ε_{Nd} of −53) tend to yield ε_{Nd} values that are too low at a given *mg*-number, whereas AFC with a Proterozoic

Table 3: Nd and Sr isotopic composition of CFB-hosted crustal xenoliths from Muren area, Vestfjella

Sample	Rock type	$^{147}Sm/^{144}Nd$	$^{143}Nd/^{144}Nd$ (180 Ma)	ε_{Nd}	T_{DM}* (Ga)	$^{87}Rb/^{86}Sr$	$^{87}Sr/^{86}Sr$ (180 Ma)	ε_{Sr}
X3-AVL-94	granitoid	0·0635	0·509834 ± 5	−51·7	3·27	0·3938	0·709965 ± 13	+63·5
X4-AVL-94	granitoid	0·0591	0·509765 ± 7	−53·0	3·24	0·3897	0·709603 ± 9	+58·5
X5-AVL-94	sandstone	0·1193	0·512078 ± 7	−9·2	1·55	0·3868	0·716362 ± 10	+154·6

Analytical description is given in Table 2.
*Depleted mantle model age (DePaolo, 1981*a*).

contaminant accords fairly well with the data. It should be noted that the Nd content (4·4 ppm) of the xenolith X4-AVL is significantly lower than that of typical Archaean rocks from the Kaapvaal (Hunter *et al.*, 1992). If a higher Nd value of 11 ppm (average of Kaapvaal trondhjemites; Table 4) is used for the contaminant (model A2; Fig. 14b), Archaean crustal material with ε_{Nd} of −53 turns out to be unsuitable for AFC modelling of the CT3 basalts.

The isotopic data of CT1 are controversial. The low ε_{Nd} values of CT1 indicate a Precambrian LREE-enriched lithospheric component in these rocks. A plot of ε_{Nd} with *mg*-number (Fig. 14a) demonstrates that the ε_{Nd} values are rather scattered and do not show evidence of simultaneous fractionation and assimilation of Archaean crust. In fact, incorporation of Proterozoic crustal material with ε_{Nd} higher than −15 would better explain why the ε_{Nd} values of some evolved CT1 are relatively high. These samples, however, also exhibit the lowest ε_{Sr} in contrast to the expected AFC relationship with a Proterozoic contaminant (Fig. 14b). The isotopic data for CT1 thus do not show clear evidence of AFC and are somewhat more accordant with a model in which the degree of crustal contamination is inversely related to the degree of fractionation of the basalt magmas (see Devey & Cox, 1987). In this case the increase in SiO_2 and decrease in Sm/Nd should have been caused by some other differentiation process, such as magma mixing in a periodically refilled and tapped magma chamber (O'Hara, 1977). It is also possible that the isotopic variations of primitive CT1 were large enough to mask isotopic evidence of AFC in the daughter magmas.

We conclude that the relatively high SiO_2, low Sm/Nd and negative ε_{Nd} values of evolved CT3 reflect an AFC process. On the basis of Nd isotopic evidence, the most likely contaminant is crustal material derived from the Proterozoic Maud Belt. Available isotopic data for the CT1 tholeiites are contradictory. On the basis of coupled increase in SiO_2 and pronounced decrease in Sm/Nd, AFC was probably involved in their evolution, although the isotopic compositions do not show clear AFC relationships. The high-*mg*-number CT1 lavas already exhibit the diagnostic features of CT1 with distinctly low ε_{Nd} and a geochemical affinity to crustal material.

Differentiation of CT2

As a whole, CT2 shows minor decrease in Sm/Nd consistent with simple gabbroic fractionation or AFC with low rate of assimilation (Fig. 12b). The CT2 suite A and suite B lavas and the CT2 dykes, however, include primitive, high-*mg*-number samples as well as evolved samples (Fig. 13a) and seem to record at least three separate batches of magma, each of which fractionated differently. The sill rock with ε_{Nd} of +7·6 could be considered as a separate subtype of intrusive CT2, but because evolved, isotopically similar rocks have not been found, the sill rock is excluded from this part of discussion. On the basis of its isotopic composition, the lava flow P55-AVL at 800 m level is included here in suite A in spite of its stratigraphic position and high SiO_2 (Fig. 6, Table 1).

The CT2 dyke rocks with high and low *mg*-number have similar positive ε_{Nd} values, suggesting that AFC was not operating (Fig. 13a). On the other hand, the decrease in ε_{Nd} from +0·3 to −2·2 in the CT2 suite A and from −6·7 to −7·5 in the CT2 suite B with decreasing *mg*-number indicates that AFC probably played a role in their differentiation. An AFC model with low rate of assimilation ($r = 0{\cdot}05$) and an Archaean contaminant akin to average Kaapvaal trondhjemite (Table 4) with ε_{Nd} (180 Ma) of −53 can successfully explain the isotopic variations and the lack of pronounced changes in Sm/Nd of suite A (Figs 12b and 13a). A similar model could also account for the isotopic variations of suite B. The role of crustal contamination in generating three isotopically different suites of CT2 (Fig. 14a) is a subject of further discussion.

Generation of different magma series

The chemical and Nd and Sr isotopic variations of the Vestfjella magma types evidence crustal contamination

Table 4: Major (wt %) and trace element (ppm) composition of possible crustal contaminants

	X4-AVL	AGS	UC
SiO_2	73·64	72·85	66·00
TiO_2	0·15	0·22	0·50
Al_2O_3	15·34	15·21	15·20
FeO_{tot}	1·26	1·45	4·50
MnO	0·02	0·02	0·08
MgO	0·68	0·38	2·20
CaO	2·61	1·95	4·20
Na_2O	5·33	5·12	3·90
K_2O	1·26	2·15	3·40
P_2O_5	0·03	0·06	0·40
LOI	n.d.	0·74	n.r.
Total	100·32	99·43	100·38
Ba	383	401	550
Rb	27	68	112
Sr	568	509	350
Zr	76	131	190
Sc	4	2·8	11
Nb	1·85	7·0	25
Y	1·05	10·0	22
Th	0·08	n.r.	10·7
U	0·13	n.r.	2·8
La	13·16	13·81	30
Ce	17·41	20·74	64
Pr	1·47	2·86	7·1
Nd	4·41	11·42	26
Sm	0·49	1·80	4·5
Eu	1·10	0·50	0·9
Gd	0·31	2·97	3·8
Tb	0·04	1·80	0·64
Dy	0·21	0·38	3·5
Ho	0·04	n.r.	0·80
Er	0·10	1·12	2·3
Tm	0·02	n.r.	n.r.
Yb	0·10	0·73	2·2
Lu	0·02	n.r.	0·32

X4-AVL is basalt-hosted xenolith from Muren, Vestfjella. AGS and UC are a 3·27 Ga Anhalt Granitoid Suite trondhjemite (average of eight samples; Hunter *et al.*, 1992) and average upper crust of Rudnick & Fountain (1995), respectively. n.d., not determined; n.r., not reported.

associated with fractional crystallization. A key question in regard to the origin of the four magma series is whether they could represent differentiates of a common parental magma.

Parental magma composition

Few of the analysed basalts could be safely regarded as uncontaminated mantle-derived material. On the basis of their OIB-like geochemistry, positive ε_{Nd} (+3·6) and low ε_{Sr} (+1), the CT4 dykes (Luttinen *et al.*, 1998) are not considered to be crustally contaminated. They are too enriched in incompatible elements, however, to represent parental magma for the other three basalt types. The high ε_{Nd} (+7·6), low ε_{Sr} (−16) and MORB-like incompatible element signature of the CT2 sill sample P27-AVL suggest that it may closely correspond to an uncontaminated asthenosphere-derived parental magma type. On the basis of its moderate *mg*-number (0·61), it hardly represents unfractionated primary magma. Correction for ~30% of olivine fractionation (by adding olivine) yields a feasible primitive magma composition that could have been in equilibrium with a mantle peridotite. Concentrations of the incompatible elements have been corrected accordingly to generate a hypothetical parental magma for petrogenetic modelling (Table 5). The CT2 sill sample exhibits positive Ba, K and Sr anomalies in Fig. 5. Hydrothermal alteration may have affected the LILE contents of this rock sample and, consequently, the composition of the hypothetical CT2 parent is poorly constrained with respect to mobile elements. None the less, it is possible that the high Ba/Nb and Sr/Nd ratios reflect a primary magma composition resembling LILE-enriched MORB from the Southwest Indian Ocean Ridge (Le Roex *et al.*, 1989; see also Luttinen *et al.*, 1998).

Crustal contamination

Comparison of CT1, CT2 and CT3 demonstrates that if a common parental magma type is assumed for them, each magma series requires a different kind of crustal contaminant to explain, for example, the different combinations of Nb, Ta, P and Ti anomalies shown in Fig. 15.

In the case of CT1, the key question is the origin of the common CT1 signature, which is characterized by features that are typical of crustal material. A similar signature typifies low-Ti CFBs world-wide and the role of crustal contamination in the origin of CFBs has remained a major controversy. Arndt *et al.* (1993) pointed out the advantages of an assimilating RTF (replenished–tapped–fractionating) magma system (O'Hara, 1977) compared with a simple AFC process (see Hergt *et al.*, 1991) and showed that low-Ti CFBs could be generated from MORB-like parental magmas in a periodically refilled magma chamber. The remaining problematic aspect of crustal contamination models is that they invariably suggest a large amount (20–30 wt %) of crustal component in the low-Ti CFBs (e.g. Arndt *et al.*, 1993; Peng *et al.*, 1994; Luttinen *et al.*, 1998). In our mind, this is difficult to reconcile with the overall homogeneity and

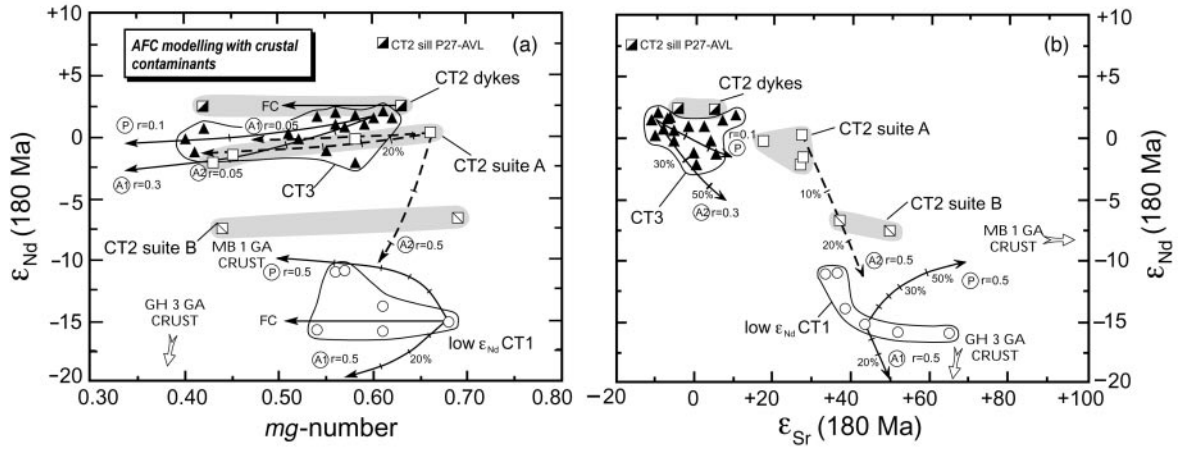

Fig. 14. Modelling of ε_{Nd} and (a) *mg*-number and (b) ε_{Sr} variations as a result of low-pressure differentiation of CT1, CT2 and CT3 magma types. The arrow (FC) in (a) indicates 50% fractionation of olivine (20%), clinopyroxene (30%) and plagioclase (50%) with bulk *D* values for Nd of 0·12 and 0·94, respectively. AFC models with the same fractionate but different crustal contaminants and *r* values are indicated. Tick marks show 10% intervals of degree of fractionation. Mixing endmembers for CT1, CT2 and CT3 are the same as in Fig. 13 apart from ε_{Sr} of CT3, for which a representative value of −10 has been used. Contaminants A1 and A2 represent Grunehogna craton (GH 3 Ga crust), whereas P is Proterozoic Maud Belt crust (MB 1 Ga crust). A1 is xenolith X4-AVL (ε_{Nd} −53, ε_{Sr} +63), A2 is isotopically similar, average Archaean trondhjemite from Kaapvaal, Africa, and P (ε_{Nd} −8, ε_{Sr} +132) is a hypothetical Proterozoic crustal contaminant (Tables 3 and 4). Data sources: Luttinen *et al.* (1998); this work.

large volume of low-Ti CFB suites and the lack of associated silicic magmatism.

The most plausible environment for extensive contamination and efficient homogenization to occur is in large magma chambers at the base of the crust, where primitive, high-density precursors of low-Ti CFBs are likely to be trapped (Cox, 1980). The lower continental crust is chemically similar to low-Ti CFBs (Rudnick & Fountain, 1995) and bulk assimilation of such material is not efficient in modifying the composition of basalt magmas. Prolonged underplating of basalt magmas, however, could have led to substantial melting of the lower crust and bimodal magmatism (e.g. Huppert & Sparks, 1988). A world-wide and well-documented example of voluminous continental bimodal magmatism is provided by the Proterozoic rapakivi associations (e.g. Haapala & Rämö, 1992). Despite the apparently favourable conditions for major mixing processes to occur, effective mixing of the basaltic and granitic magmas in the rapakivi systems has been limited (Rämö, 1991). The rare examples of interaction between the silicic and mafic magmas demonstrate that magma mingling was the predominant process as a consequence of the contrasting physicochemical characteristics of the mixed endmembers (Salonsaari, 1995).

Assuming, however, that bimodal magmatism and effective magma mixing was required to generate the CT1 lavas and other low-Ti magma types of the Karoo province, some of the low-density anatectic melts should presumably have avoided mixing with the basalts. It is difficult to explain the absence of eruptive and intrusive manifestations of coeval and voluminous silicic magmatism associated with the low-Ti lavas of Dronning Maud Land and southeast Africa. The voluminous Karoo rhyolites of the Lebombo Monocline post-date the main stage of CFB magmatism and they have been interpreted to record remelting of underplated Jurassic (low-Ti?) CFBs (Harris & Erlank, 1992; Cox, 1993).

Finally, a well-adjusted mixing process would be required to explain why all the CT1 basalts include a large and practically constant amount of crustal component as demonstrated by the similar size of the negative Ti anomalies (Fig. 15). Such conditions would characterize an ideal steady state of an assimilating RTF system (O'Hara, 1977; Arndt *et al.*, 1993), but the randomness expected in natural systems should have led to compositional gradation between the mixed endmembers as a result of occasional tapping and eruption of moderately contaminated magmas (see Cox, 1988). This is strongly contrasted by the common CT1 signature of the lavas with *mg*-number above 0·65. Such primitive basalts could hardly represent steady-state magma compositions. In sum, generation of low-Ti CFB types, such as CT1, by crustal contamination can be numerically modelled with a combined AFC and RTF process, but such a model is undermined by some critical general geological arguments.

The heterogeneous CT2 lavas and dykes record a strongly differentiated suite of CFB magmas that were probably derived from the same MORB-like parental magma type. Here we focus on the marked difference

Table 5: Lithospheric mantle contamination modelling of CT1 and CT2; immobile incompatible elements (ppm)

	Th	Ta	Nb	Ce	Pr	Nd	P	Hf	Zr	Sm	Eu	Ti	Gd	Tb	Ho	Y	Yb	Lu	Sr*	ε_{Sr}	ε_{Nd}
Contaminant†	32	6·3	135	470	35	157	5673	32	1160	23	5·1	24580	12·7	1·6	1·0	20	1·7	0·23	3500	+100	−25
Parental CT1‡	0·24	0·17	2·93	12·28	1·66	7·77	500	1·74	67	2·28	0·83	4494	2·52	0·43	0·52	13	1·08	0·16	176	+9	−2·5
Parental CT2‡	0·16	0·12	2·19	8·55	1·37	7·37	458	1·72	60	2·70	1·0	7428	3·04	0·55	0·64	15·4	1·21	0·18	133	−16	+7·5
20% AFC of CT1§	1·19	0·39	7·40	28·4	3·04	14·00	781	3·06	116	3·48	1·18	6271	3·50	0·58	0·68	16·8	1·39	0·21	317	+37	−9·5
30% AFC of CT2§	0·95	0·31	6·16	22·7	2·74	14·02	780	3·17	112	4·36	1·54	11084	4·61	0·82	0·93	22·4	1·76	0·26	268	+18	−0·7

*Sr concentrations of lamproite and parental CT2 were modified to fit the immobile element modelling (see text for details).
†Lamproitic contaminant from lithospheric mantle of Grunehogna craton. Composition is the average of Rock (1991).
‡Hypothetical parental magmas were calculated assuming that the average of high-ε_{Nd} CT1 corresponds to 50% of olivine fractionation of the parental CT1 and that CT2 sill rock P27-AVL is the result of 30% of olivine fractionation of parental CT2 (see Fig. 15).
§AFC models were calculated using the equations of DePaolo (1981*b*) assuming olivine fractionation and bulk *D* values of 0·01 for all elements (0·02 for Ti) (see Rollinson, 1993). Rates of assimilation used for CT1 and CT2 were 0·1 and 0·05, respectively. Model results and measured data for CT1 and CT2 are compared in Figs 15 and 16.

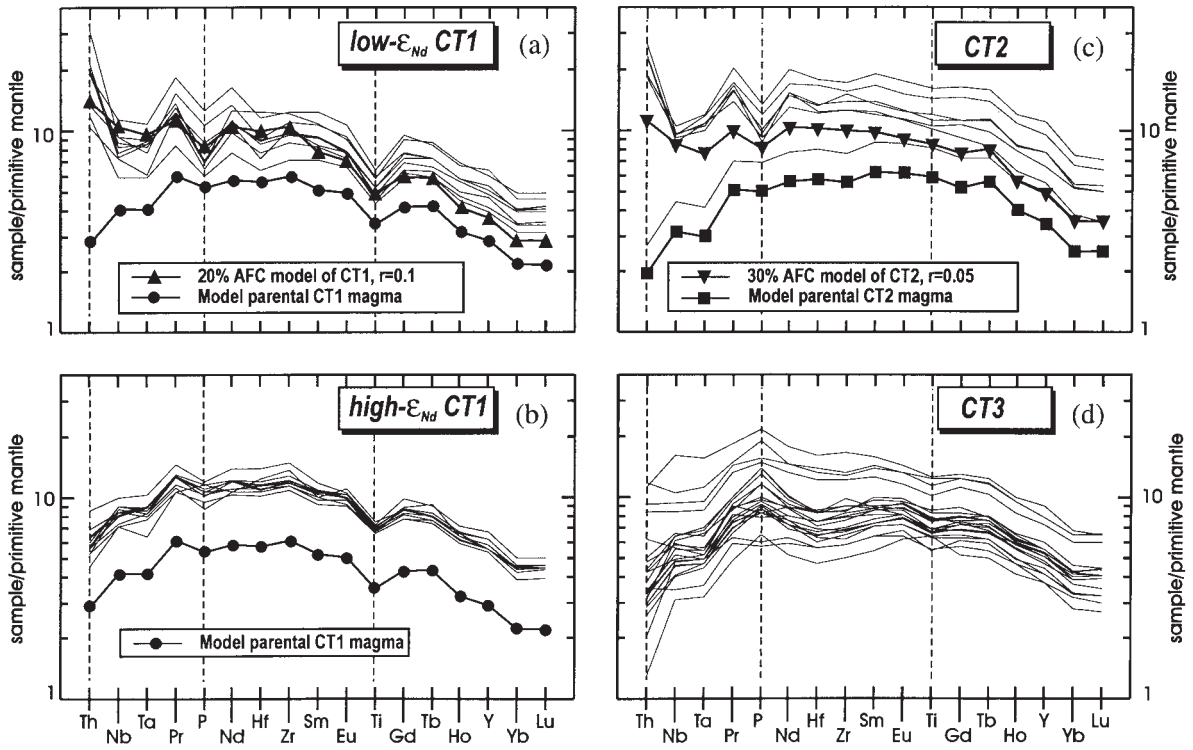

Fig. 15. Primitive mantle-normalized immobile incompatible element diagrams of (a) low-ε_{Nd} CT1, (b) high-ε_{Nd} CT1, (c) CT2 and (d) CT3 rocks. Lithospheric contamination models and hypothetical primary magmas of CT1 and CT2 (Table 5) are shown. Lithospheric contaminant is average lamproite of Rock (1991) (Table 5). Dashed lines point to diagnostic anomalies of CT1, CT2 and CT3.

between the high-*mg*-number CT2 lavas and the hypothetical CT2 parental magma, which is demonstrated first and foremost by the lower ε_{Nd}, $(P/Nd)_n$ and higher $(Th/Ta)_n$ of the lavas (Figs 12 and 15). Considering the relatively low SiO_2 and $(La/Sm)_n$, and high $(Ti/Gd)_n$ and *mg*-number recorded by the suite A lavas, these differences point to a contaminant that (1) was not particularly high in SiO_2, (2) was strongly enriched in LREE but not in HREE relative to parental CT2 and (3) exhibited a strong negative P anomaly but not a corresponding negative Ti anomaly. These features are not considered to be typical of crustal-derived material and the wide compositional ranges of the high-*mg*-number CT2 are more consistent with a mafic incompatible element enriched contaminant.

The similarity of the incompatible element signatures of the suite A and B lavas (Figs 5b and 15) implies that the cause of high SiO_2 of suite B was not directly linked to the development of the trace element patterns. The high SiO_2 strongly suggests a crustal component in suite B and its isotopic compositions can be modelled reasonably well by crustal contamination of primitive CT2 suite A magmas with an Archaean trondhjemitic contaminant (Table 4) and assimilation rate of 0·2 (Fig. 14).

The CT3 lavas show some affinities to CT1 and the other Karoo low-Ti CFBs but also to CT2. Geochemical indications of significant crustal contamination, such as high SiO_2, $(La/Sm)_n$, $(Th/Ta)_n$ and ε_{Sr}, and low $(P/Nd)_n$, $(Ti/Gd)_n$ and ε_{Nd}, are lacking in the high-*mg*-number CT3 lavas. In terms of immobile incompatible elements and the Nd and Sr isotopic ratios, the high-*mg*-number CT3 lavas show affinities to MORB and resemble the hypothetical parental CT2 magma (Figs 14 and 15). On the other hand, relatively high $(P/Nd)_n$ of CT3 is not a typical result of crustal contamination and suggests that the parental magma of CT3 was somewhat different from that of CT2.

Although crustal contamination influenced the low-pressure fractionation of the CT1, CT2 and CT3 magmas it does not seem to have been responsible for the generation of the different magma series. An important common feature of the Vestfjella magma types is that each of them includes rocks with notably high *mg*-number, indicating that relatively primitive magmas already exhibited the diagnostic incompatible element and isotopic signatures of CT1, CT2, CT3 and CT4. We consider that the magma types possessed their salient features essentially before emplacement into the crust.

Lithospheric mantle contamination

A possible mechanism that could have led to contamination of basalt magmas before they reached the crustal level is mixing with small-degree melts of lithospheric mantle (McKenzie, 1989; O'Brien *et* al., 1991; Ellam & Cox, 1991; Ellam *et al.*, 1992; Foley, 1992; Cadman *et al.*, 1995). Subcontinental lithospheric mantle may include domains characterized by abundant veins rich in clinopyroxene and mica and/or amphibole. These veins typically have lower solidus temperatures than their wall-rock peridotite and incipient melting of such veined lithosphere is likely to produce highly alkaline melts, such as lamproites (McKenzie, 1989; Foley, 1992). Melting modelling of a vein-derived component would be complicated because of uncertainties with respect to the mineralogical and chemical composition of the vein assemblage, solid-solution melting reactions and dissolution of the wall-rock minerals (Foley, 1992). Instead, we have used the average lamproite of Rock (1991) to approximate a hypothetical vein-derived component.

Previously, Luttinen *et al.* (1998) speculated on whether the CT1 basalts could have been generated by mixing of MORB-like asthenosphere-derived magmas and lithosphere-derived lamproitic material. Although such a lithospheric mantle contamination model could explain many of the characteristic features of CT1, including the low Ti/Zr, it would, at the same time, lead to a strong enrichment of the highly incompatible elements and, for example, notably higher $(Nb/Y)_n$ than those recorded by primitive CT1 (see Luttinen *et al.*, 1998). We conclude that lithospheric mantle contamination is an improbable explanation for the common CT1 signature and the origin of the CT1 magma type. Detailed examination of the trace element characteristics of the CT1 and CT2 suites shows that such a process presumably played an important role in generating subtypes of CT1 and CT2, however.

Trace element constraints on lithospheric mantle contamination

Compared with the CT2 sill, the CT2 lavas have higher LREE, $(Th/Ta)_n$ and ε_{Sr}, and lower $(P/Nd)_n$ and ε_{Nd} values (Figs 14 and 15). Importantly, a similar result is obtained when comparing the high-ε_{Nd} and low-ε_{Nd} CT1 rocks. In spite of their different overall compositions, the CT1 and CT2 suites seem to have incorporated the same enriched component, which influenced the highly incompatible element ratios but caused minor changes in the major elements and moderately incompatible element ratios, such as $(Ti/Gd)_n$. Here we examine whether lithospheric mantle contamination could have produced the low-ε_{Nd} subtypes of CT1 and CT2. The high-ε_{Nd} CT1 rocks have relatively low *mg*-number (<0·6). For the modelling, a hypothetical parental high-ε_{Nd} CT1 magma has been calculated in a similar fashion as previously was done in the case of CT2 (Table 5).

In the lithospheric mantle contamination model (Fig. 15), the hypothetical parental CT1 and CT2 magmas crystallized olivine as they were emplaced into a subcontinental lithosphere and mobilized and entrained highly enriched melts from the veined wall-rock mantle. The process has been modelled using the AFC equations of DePaolo (1981*b*). The bulk *D* values were assumed to be 0·01, with the exception of the value of Ti, for which 0·02 was used in accordance with olivine fractionation (Rollinson, 1993). AFC modelling with a contaminant similar to the average lamproite of Rock (1991) demonstrates that lithospheric contamination with low assimilation rates could account for the different immobile element patterns of high-ε_{Nd} and low-ε_{Nd} subtypes of both CT1 and CT2 (Fig. 15).

Isotopic constraints on lithospheric mantle contamination

Lithospheric mantle contamination would strongly have influenced also the isotopic compositions if the lamproitic component had been derived from an ancient reservoir with low Sm/Nd and high Rb/Sr relative to chondrite. Archaean crust and mantle ages for the Kaapvaal craton show long-term physical coupling of mantle and crust over a 3 Gy period (Pearson *et al.*, 1995). The xenolith data (Table 3) thus suggest that Archaean, cratonic lithospheric mantle may well extend beneath or at least close to the Vestfjella region (Fig. 1). Kimberlite-hosted peridotite and mineral inclusions provide evidence for the composition of the Kaapvaal lithospheric mantle (Menzies & Murthy, 1980; Richardson *et al.*, 1984; Walker *et al.*, 1989; Pearson *et al.*, 1995) and give the best estimate of the cratonic lithosphere in western Dronning Maud Land. The isotopic variations indicate considerable heterogeneity with, for example, ε_{Nd} at 180 Ma ranging from -4 to -32 (Richardson *et al.*, 1984). As a consequence of successive infiltration of depleted Archaean Kaapvaal mantle by various asthenosphere-derived melts, the Kaapvaal–Grunehogna lithospheric mantle probably records intermediate compositions between DM, EM1 and EM2 mantle components (see Zindler & Hart, 1986) as demonstrated by the enriched mantle array of Menzies & Murthy (1980) (Fig. 16b; Menzies, 1990).

We assume that the purported lamproitic component showed an isotopic affinity to the enriched mantle array. Trace element model parameters can be used to constrain the isotopic composition of this component: a contaminant with ε_{Nd} (180 Ma) of -25 complies reasonably well with the trace element AFC modelling of the low-ε_{Nd} CT1 as well as the CT2 lavas (Fig. 16a). Modelling of the Sr isotopic systematics is more complicated because of uncertainties with respect to possible alteration effects. This problem is particularly significant in the case of

CT2 because a single sample was used for deriving the parental magma composition (Table 5). The CT2 sill rock sample shows a positive Sr anomaly with Sr/Nd of 21, which is substantially higher than the corresponding ratio for average depleted MORB (~12, Sun & McDonough, 1989). Here we assume that before alteration the sill rock had a somewhat lower Sr/Nd of 18 corresponding to Sr content of 133 ppm for the hypothetical primary CT2 magma. A lamproitic contaminant with ε_{Sr} (180 Ma) of +100 shows isotopic affinity to the enriched mantle array and would reasonably well explain the Sr isotopic ranges of both CT1 and CT2 suites (Fig. 16b). It would be possible to explain the isotopic compositions of the CT2 suite B lavas by lithospheric mantle contamination alone. The high SiO_2 of suite B lavas, however, strongly suggests that these rocks contain a significant crustal-derived component. The Sr concentration (3500 ppm) and thus the Sr/Nd ratio (22) used for the model are clearly higher than those of the average lamproite (1250 ppm and 8, respectively), but Sr contents of >4000 ppm and Sr/Nd ratios up to 24 have been reported for lamproites and related rock types (e.g. Rock, 1991; Larsen & Rex, 1992).

In the isotopic modelling, the Sr concentrations of the CT2 parental magma and the lamproite were adjusted so that the same contaminant could explain the variations of both CT1 and CT2 magma series. Overall, the modelling serves to illustrate the feasibility of lithospheric mantle contamination in explaining not only the chemical (Fig. 15) but also the isotopic ranges of the CT1 and CT2 suites (Fig. 16). The composition of the vein-derived lithospheric mantle component is poorly constrained and the contaminant could well have been even more enriched in incompatible elements than lamproites, which have been considered as mixtures of the vein and wall-rock mantle material (e.g. Foley, 1992). In that case our calculations would overestimate the lithospheric mantle contribution to the CT1 and CT2 magmatism.

Sublithospheric and lithospheric mantle sources

On the basis of their positive ε_{Nd} values and chemical affinities to MORB and OIB, CT2 and CT4 probably had asthenospheric sources. The isotopic and chemical MORB affinities of the CT3 lavas are contrasted by their notably high LILE contents (Fig. 5). This selective LILE enrichment is difficult to reconcile with crustal or lithospheric mantle contamination, which is expected to lead to concomitant increase in LREE and LILE concentrations. The chemical data for CT3 thus point to a strongly LILE-enriched source composition.

The origin of low-Ti CFBs, such as CT1, has been often ascribed to lithospheric mantle sources (e.g. Hawkesworth *et al.*, 1984; Sweeney & Watkeys, 1990). In the same vein, Luttinen *et al.* (1998) proposed a lithospheric source for the low-ε_{Nd} CT1. The lithospheric mantle contamination model, however, provides a feasible explanation for derivation of the low-ε_{Nd} CT1 type from high-ε_{Nd} type CT1 parental magmas. Nevertheless, it cannot account for the invariably high SiO_2 and the negative Ti anomalies, that is, the common signature of CT1, which seem to require a lithospheric source for this magma type (see Turner & Hawkesworth, 1995). It is possible to invoke a layered lithospheric mantle with a deeper source for high-ε_{Nd} type parental magmas of CT1 and an overlying veined domain where these magmas were contaminated to produce low-ε_{Nd} CT1. The data for high-ε_{Nd} CT1 may thus reflect the characteristics of the primary source of CT1 magmas.

Comparison of the high-ε_{Nd} CT1 and CT3 shows them to have rather similar incompatible element signatures (Figs 5, 11 and 15). Here we discuss possible links between the sources of these low-Ti magma series. There has been frequent speculation on possible connections between the sources of Gondwana low-Ti CFBs and subduction processes (e.g. Hergt *et al.*, 1991; Brewer *et al.*, 1992). For example, Duncan (1987) has shown that the low-Ti tholeiites of south Lebombo plot within the calc-alkaline fields of the Ti–Zr–Y and Ti–Zr–Sr diagrams of Pearce & Cann (1973). The chemically similar CT1 also exhibits these affinities to calc-alkaline volcanic rocks, whereas CT3 would plot mainly in the low-K tholeiite fields of the above-mentioned diagrams.

In their discussion on the origin of the Gondwana low-Ti CFBs, Hergt *et al.* (1991) calculated that a geochemically suitable low-Ti source with a crust-like trace element signature could have been generated by incorporation of a minor quantity of sediment material in depleted Gondwanan upper mantle during subduction. Such a source would explain the crust-like features of the parental CT1 lavas. In volcanic arc systems, the composition of the subduction-contaminated mantle wedge can vary substantially depending on, for example, the amount of subducted sediment and whether the slab-derived component is generated by dehydration or partial melting. Previously, Luttinen *et al.* (1998) proposed that the selective LILE enrichment of CT3 reflects a subduction-influenced source of this magma type. The enrichment of P (Fig. 15) lends support to this interpretation because subduction-liberated fluids and melts may effectively increase LILE, LREE and also P contents in the overlying mantle wedge and, at the same time, cause only small changes in most HFSE and middle to heavy REE concentrations (Tatsumi *et al.*, 1986; Pearce & Peate, 1995; Pearce *et al.*, 1995).

In conclusion, the Jurassic mantle source regions of CT1 and CT3 and those of island arc basalts have marked similarities. In the case of CT1 and CT3, such

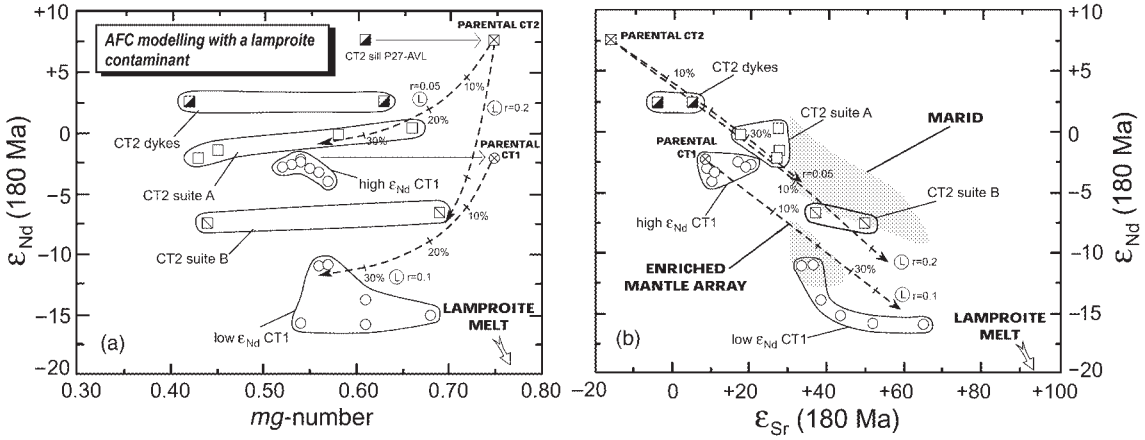

Fig. 16. Modelling of initial ε_{Nd} and (a) *mg*-number and (b) ε_{Sr} variations as a result of lithospheric contamination of CT1 and CT2 magma types. AFC models with primary CT1 and CT2 (Table 5) and a lamproitic contaminant (L) (Table 5) (ε_{Nd} −25, ε_{Sr} +100, *mg*-number 0·83) are indicated. Tick marks indicate 10% intervals of degree of fractionation. Shaded fields in (b) show compositions of the Kaapvaal enriched mantle array (Menzies & Murthy, 1980) and MARID (mica–amphibole–rutile–ilmenite–diopside) xenoliths (Kramers *et al.*, 1983; Waters, 1987). Data sources: Luttinen *et al.* (1998); this work.

a source could have been generated in association with subduction-related contamination of the upper mantle during two distinct periods. First, the Proterozoic lithospheric terrane of Dronning Maud Land is an accretionary volcanic arc complex (Groenewald *et al.*, 1995). It is possible that the associated upper mantle could have been variably contaminated by subducted sediments and slab-derived fluids and melts to produce a laterally heterogeneous source for CT1 and CT3. Second, researchers have also speculated on whether Jurassic subduction along the proto-Pacific margin of Gondwana could have influenced the break-up magmatism (e.g. Cox, 1978; Elliot, 1990). The Karoo igneous province, however, was separated by >2000 km from the active Jurassic subducting margin. An extremely flat subduction angle would have been required to extend subduction-related mantle contamination to the source regions of CT1 and CT3 (cf. Murphy *et al.*, 1998; Dalziel *et al.*, 1999). We prefer that the assumed subduction-contamination preceded the break-up magmatism and was not directly linked to it. An LILE- and LREE-enriched mantle domain could have been restored in the Proterozoic lithosphere or, perhaps more likely, in the sublithospheric thermal boundary layer of the Gondwanan upper mantle (see Anderson, 1994).

Magmatic plumbing systems and lithospheric thinning zones

Stratigraphic alternation of the compositionally distinctive CT1, CT2 and CT3 magma series strongly implies coexistence of three different magmatic plumbing systems. On the basis of Nd isotope compositions, CT1 and CT2 were contaminated with Archaean and the CT3 lavas by Proterozoic lithospheric material. Accordingly, lavas with notably low ε_{Nd} values occur only in the north Vestfjella and palaeoflow direction measurements indicate that they flowed mainly from north to south, i.e. from an area of Archaean lithosphere (Fig. 17). Lavas with near-chondritic ε_{Nd} are predominant toward the southern Vestfjella (Fig. 17). On the basis of flow directions, their source regions were located east and south of Vestfjella. Overall, there is a good correlation between the apparent source regions of the CFBs with high and low ε_{Nd} and the distribution of the Archaean and Proterozoic terranes of the Dronning Maud Land lithosphere (Fig. 17). This is accordant with two main magmatic plumbing systems; one within the Grunehogna craton and the other within the Maud Belt. Development of two active lithospheric thinning zones probably had a controlling influence on these systems.

The Lebombo magmatism of Africa has been ascribed to thinning in the Mozambique–Weddell Sea zone (Figs 1 and 17) (e.g. Cox, 1992). Similarly to the Lebombo lavas, the Vestfjella CFBs are located close to the present continental margin and were spatially associated with the Mozambique–Weddell Sea zone. Another major rifting regime related to the Gondwana break-up in western Dronning Maud Land is expressed by the Jutulstraumen–Pencksökket (Jutul–Penck) trough (e.g. Marsh, 1991) (Fig. 17) along which alkaline magmatism occurred at 180 Ma (Grantham & Hunter, 1991; Harris & Grantham, 1993; Grantham, 1996). Seismic measurements have defined a similar graben-like structure extending to the southwest from Pencksökket, parallel to Heimefrontfjella (Hungeling & Thyssen, 1991). Although extensive in some localities, this 'failed' off-cratonic rifting did not lead to an oceanic spreading centre (Spaeth, 1987), whereas lithospheric

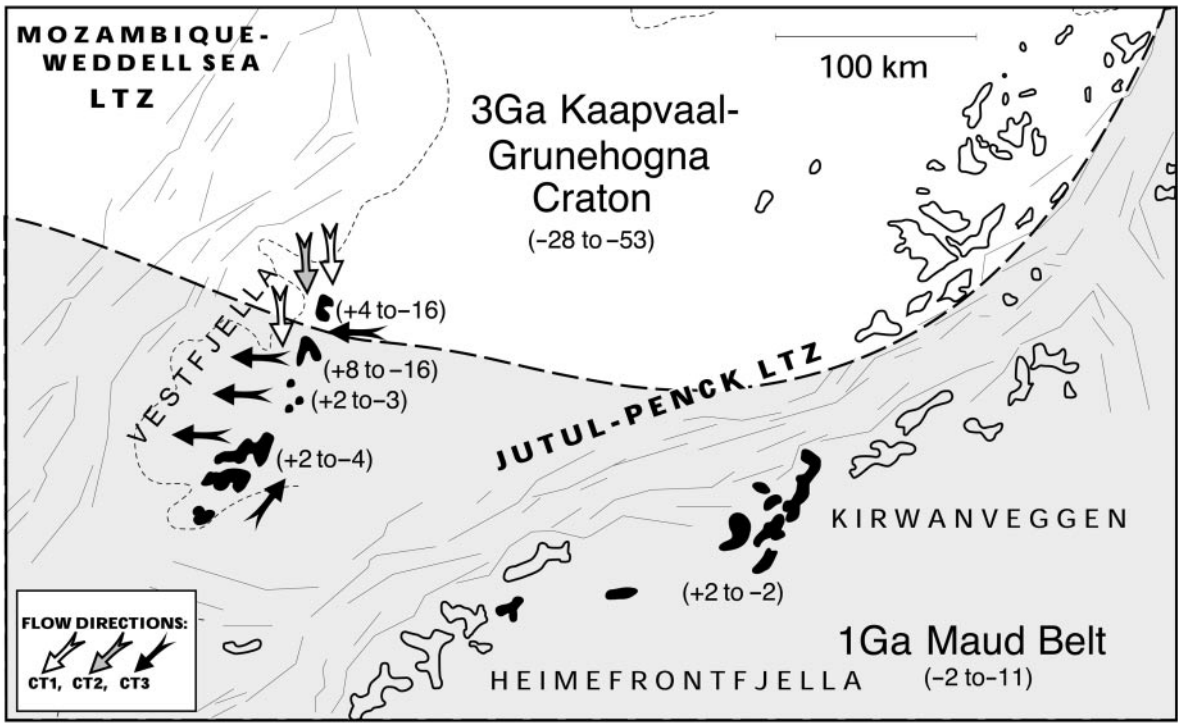

Fig. 17. Distribution of the Jurassic CFBs (black), Archaean (Kaapvaal–Grunehogna) and Proterozoic (Maud Belt) lithospheric terranes, and lithospheric thinning zones (Jutul–Penck LTZ and Mozambique–Weddell Sea LTZ) in western Dronning Maud Land. Arrows indicate predominant palaeoflow directions of CT1, CT2 and CT3 in different areas. Numbers in parenthesis show ε_{Nd} (180 Ma) values for CFBs and felsic crustal rocks. Data sources: Carlson *et al.* (1983); Arndt *et al.* (1991); Harris *et al.* (1991); Luttinen *et al.* (1998); this work.

extension in the Mozambique–Weddell Sea zone finally split the Archaean craton and developed into an ocean-floor spreading regime.

The origin of the heterogeneous Vestfjella CFB suite probably involved two major magmatic plumbing systems in areas of lithospheric thinning. Not only may lithospheric thinning zones have permitted the emplacement of magmas; also, the plume-generated thermal anomaly could have been channelled and magma production localized in such areas (Thompson & Gibson, 1991; Gallagher & Hawkesworth, 1992; Ebinger & Sleep, 1998).

Model of Vestfjella CFB magmatism

Here we propose a tectono-magmatic model for the Vestfjella CFBs. The essential components of the model include: (1) the Archaean Grunehogna craton with enriched, veined lithospheric mantle roots; (2) the Proterozoic Maud Belt terrane; (3) a variably LREE- and LILE-enriched, subduction-modified (sublithospheric?) upper-mantle source; (4) two lithospheric thinning zones—the Weddell Sea zone within the Archaean craton and the Jutul–Penck zone within the off-cratonic Proterozoic terrane.

The tectono-magmatic model is illustrated in Fig. 18. Plume–lithosphere interactions generated two lithospheric thinning zones, which controlled melting of the hot upper mantle and permitted emplacement of the generated magmas (Fig. 18a). The CT1 primary magmas were generated in an LREE- and LILE-enriched upper mantle. Most of these magmas were emplaced into a cratonic segment of the Weddell Sea lithospheric thinning zone and incorporated incompatible element enriched low-ε_{Nd} material from veined lithospheric mantle giving the ascending magmas the low-ε_{Nd} CT1 signature. Some CT1 magmas (high-ε_{Nd} CT1) were not contaminated by the enriched lithosphere and maintained the CT1 source signature. They either intruded through Proterozoic lithosphere or avoided veined parts of the Archaean lithosphere (Fig. 18b). Occasionally, small batches of melts were tapped from LREE-depleted, slightly LILE-enriched upper-mantle sources (Fig. 18b). These CT2 magmas utilized the cratonic plumbing system and, similar to CT1, were variably contaminated with an Archaean lithospheric component to yield compositionally heterogeneous CT2 lavas. The CT3 magmas were generated in an isotopically depleted mantle source that was notably enriched in LILE as a result of subduction-contamination. These magmas were emplaced

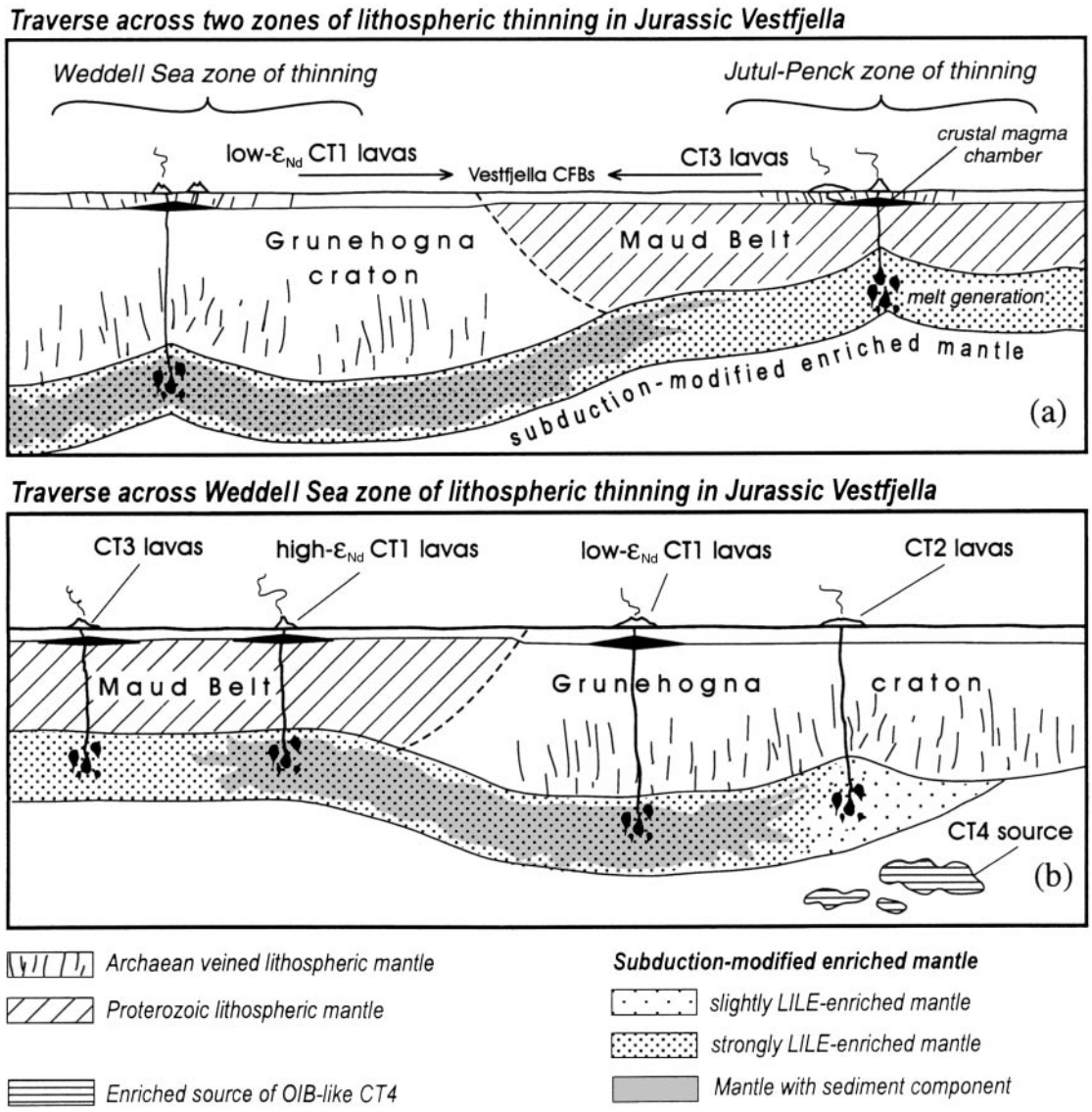

Fig. 18. A schematic presentation of Mesozoic CFB magmatism in Vestfjella region, western Dronning Maud Land, Antarctica, illustrated by traverses across two lithospheric thinning zones in Jurassic Dronning Maud Land (a) and along the Weddell Sea zone of thinning (b). Localized melting of upper mantle occurred along lithospheric thinning zones (LTZs). CT1 was generated by melting of LREE- and LILE-enriched mantle within the cratonic Weddell Sea zone (a, b). The high-ε_{Nd} type primary CT1 magmas included an Archaean LREE-enriched component as they ascended through veined lithospheric mantle and, as a consequence of this lithospheric contamination, most of the erupted basalts recorded the low-ε_{Nd} CT1 type geochemistry. CT2 primary magmas were generated in a slightly LILE-enriched, LREE-depleted mantle source below the Weddell Sea LTZ (b). Similar to CT1, they were subjected to lithospheric contamination resulting in variable low ε_{Nd} in the erupted lavas. CT1 and CT2 were further contaminated with Archaean crustal material. CT3 was derived from strongly LILE-enriched upper mantle. These magmas were emplaced into the Proterozoic lithosphere and ascended to crustal levels without significant contamination. They were contaminated, however, with Proterozoic crust in crustal level magma chambers. The late-stage CT4 dykes may record melting of enriched parts of asthenospheric mantle (b) (see Luttinen *et al.*, 1998). Penecontemporaneous localized melting of heterogeneous upper mantle across an Archaean–Proterozoic lithospheric terrane boundary resulted in interbedded, compositionally distinct lava flows in Vestfjella between the two lithospheric thinning zones.

into the off-cratonic lithospheric thinning zone and were not subjected to lithospheric mantle contamination.

Crustal-level contamination also modified the compositions of CT1, CT2 and CT3 suites, but in general had relatively small impact on their diagnostic trace element and isotopic ratios. Contamination is reflected by the slight decrease in ε_{Nd} values during fractionation of CT2 and CT3 lavas, whereas isotopic variations of

lithospheric mantle contaminated high *mg*-number CT1 magmas probably masked subsequent AFC relationships.

Between the two major zones of eruptive activity, the CT1, CT2 and CT3 basalts were interbedded (Figs 6 and 18). Towards the later stages of magmatism the predominant type in the cratonic zone of thinning changed to relatively uncontaminated CT2 recorded by the dyke rocks and sills. Emplacement of these MORB-like magmas was associated with occasional tapping of OIB-like compositions (CT4 dykes) from heterogeneous asthenosphere (see Luttinen *et al.*, 1998).

Mantle heterogeneity and Karoo magmatism

Our results lend support to the previously presented idea that lithospheric mantle contamination played a key role in Karoo magmatism associated with the Mozambique lithospheric thinning zone. Ellam and coworkers (Ellam & Cox, 1989, 1991; Ellam *et al.*, 1992) have suggested that the high-Ti picrites of Mwenezi area (Fig. 1) record a mixing lineage between asthenosphere-derived parental magmas and a lithospheric mantle component. Our modelling of the CT2 suite suggests that such a process operated also in north Vestfjella. Interestingly, isotopic data on MARID (mica–amphibole–rutile–ilmenite–diopside) mantle xenoliths from Kaapvaal (Kramers *et al.*, 1983; Waters, 1987) show affinity to CT2 (Fig. 16). Similar to the Mwenezi picrites and CT2, the MARID xenoliths have been interpreted to record mixing of asthenospheric and lithospheric mantle material (Kramers *et al.*, 1983) as a result of Mesozoic impact of a mantle plume on the base of the Kaapvaal lithosphere (Menzies, 1990; Konzett *et al.*, 1998). The significance of lithospheric mantle contamination is further underlined by the observation that also the low-Ti CT1 suite of Vestfjella seems to include the same overall lamproite-like component as CT2.

We have emphasized that CT1, CT2 and CT3 were derived from different mantle sources. It is possible that these sources actually reflect compositional gradation of variably subduction-contaminated Gondwanan upper mantle. In such a scenario, the source of CT2 represents uncontaminated or slightly LILE-enriched asthenosphere whereas the sources of CT3 and CT1 were successively more contaminated with slab-derived fluids and sediment material. Generation of the Kirwan basalts (Fig. 17) could also be linked to the proposed subduction-contaminated source. Similar to CT1, the Kirwan basalts may record melting of mantle with a subducted sediment component but this source was not influenced by strong LILE enrichment. In accord with Sweeney & Watkeys (1990), the subduction-contaminated sources of the low-Ti magma types were located mainly below the Proterozoic crust but, as the data on low-ε_{Nd} CT1 demonstrate, they also extended below the marginal parts of the Archaean craton. Towards the interior of the craton, the subduction overprint of the upper mantle presumably disappeared in the depleted source regions of high-Ti CFBs. The compositional gaps between the various magma types can be explained by localized thinning and partial melting of laterally heterogeneous upper mantle (Fig. 17).

CONCLUSIONS

On the basis of the presented data and discussion on the Jurassic Vestfjella CFBs we summarize the following conclusions.

Vestfjella magma types and their relationships to other Karoo CFBs

The Jurassic Vestfjella CFBs can be grouped into three main chemical types (CT1, CT2 and CT3) based on immobile incompatible trace element ratios, such as Ti/Zr and Ti/P. The CT1 lavas and dykes are rather typical Gondwana low-Ti tholeiites with a crust-like trace element signature, whereas CT2 resembles MORB and is regarded to be transitional between low-Ti and high-Ti magma types. The CT3 lavas show some affinities to low-Ti CFBs but are different from other Karoo low-Ti types.

The lava succession is cut by abundant dykes and sills, which represent intrusive equivalents to CT1, CT2 and CT3, but also include a distinctive, although minor group of CT4 dykes that represent a high-Ti magma type and show an OIB affinity. On the basis of our stratigraphic reconstruction, the Vestfjella CFB succession can be divided into three major units; the lower CT1-dominated suite, the middle CT3-dominated suite and the upper CT1-dominated suite. CT2 lavas occur as minor interbeds, mainly in the north.

CT1 and CT2 show wide ranges of Nd and Sr isotopic ratios with ε_{Nd} (180 Ma) from $+8$ to -16 and ε_{Sr} (180 Ma) from -16 to $+65$, in contrast to CT3 lavas, which record close chondritic isotopic ratios. The low-ε_{Nd} CT1 and the CT2 dykes and sill rock are chemically and isotopically notably similar to the Sabie River basalts, south Lebombo and Rooi Rand dykes, respectively. The high-ε_{Nd} CT1, the CT2 lavas and the CT3 lavas seem to be confined to Vestfjella. The CT4 dykes resemble some of the high-Ti CFBs of Ahlmannryggen and central Lebombo.

Two-stage differentiation

The large isotopic variations of the CT1 and CT2 suites reflect lithospheric mantle contamination. Emplacement

of (near) primary CT1 and CT2 magmas into veined cratonic lithosphere triggered incipient melting and led to mixing with vein-derived lamproite-like material, which overprinted the highly incompatible element and isotopic ratios of CT1 and CT2. The CT1 and CT2 lavas were also contaminated by Archaean Grunehogna crust, but this process had a relatively minor effect on their diagnostic incompatible element and isotopic ratios. CT3 records contamination by Proterozoic Maud Belt crust. Low-pressure fractional crystallization of olivine, plagioclase and augite had a controlling influence on the major element geochemistry of the magmas.

Importance of lithospheric thinning zones

The generation and emplacement of the CT1, CT2 and CT3 magmas was controlled by the development of two major lithospheric thinning zones associated with the Gondwana break-up in Jurassic Vestfjella and adjacent areas. The CT1 and CT2 magmas utilized plumbing systems developed in the Mozambique–Weddell Sea thinning zone. The magmas that were emplaced into a cratonic segment of this zone were subjected to lithospheric mantle contamination. The CT3 magmas were emplaced into the Jutul–Penck zone of thinning within the Proterozoic Maud Belt lithospheric terrane and were not contaminated with lithospheric mantle material.

Depleted and enriched mantle sources

The high-ε_{Nd} endmembers of CT1, CT2 and CT3 probably closely resemble uncontaminated mantle-derived magmas and indicate three different mantle sources. The CT2 primary magmas were derived from LREE-depleted sources, whereas data on the volumetrically preponderant CT1 and CT3 point to LREE- and LILE-enriched sources. The low-Ti types, CT1 and CT3, were generated as a result of localized melting of variably subduction-contaminated upper mantle. Overall, the depleted source of CT2 and enriched sources of CT1 and CT3 may record compositional gradation generated by subduction-contamination of upper mantle. The OIB-like CT4 dykes probably reflect asthenospheric heterogeneities that were unrelated to the proposed subduction-contamination.

In summary, we argue that the pronounced heterogeneity of the Vestfjella CFB suite is fundamentally linked to long-term evolution of the Gondwanan upper mantle associated with an Archaean–Proterozoic lithospheric terrane boundary. Generation of separate plumbing systems and melt production and contamination in compositionally different parts of such a heterogeneous mantle source may well have been controlled by the distribution and nature of lithospheric thinning zones, which related to initial rifting and the break-up of Gondwana in the western Dronning Maud Land.

ACKNOWLEDGEMENTS

We thank Eero Hanski, Raimo Lahtinen, Hugh O'Brien, Tapani Rämö and Brian Robins for their constructive comments on the manuscript. We appreciate careful analytical work by Peter Hooper, Diane Johnson and Charles Knaack at the Geoanalytical Laboratory, Washington State University, and thank Hannu Huhma, from the Geological Survey of Finland, and Tapani Rämö for Nd and Sr isotopic analysis of two samples. Reviews by Chris Harris and Martin Menzies substantially improved the paper. A.V.L. was funded by the Finnish Ministry of Education and the Academy of Finland (Grant No. 43922). Fieldwork was funded by the Finnish and Norwegian Antarctic research programmes. This is a contribution to the Lithosphere Graduate School.

REFERENCES

Anderson, D. L. (1994). The sublithospheric mantle as the source of continental flood basalts; the case against the continental lithosphere and plume head reservoirs. *Earth and Planetary Science Letters* **123**, 269–280.

Arndt, N. T., Todt, W., Chauvel, C., Tapfer, M. & Weber, K. (1991). U–Pb zircon age and Nd isotopic composition of granitoids, charnockites and supracrustal rocks from Heimefrontfjella, Antarctica. *Geologische Rundschau* **80**, 759–777.

Arndt, N. T., Czamanske, G. K., Wooden, J. L. & Fedorenko, V. A. (1993). Mantle and crustal contributions to continental flood basalt volcanism. *Tectonophysics* **223**, 39–52.

Arndt, N. T., Chauvel, C., Czamanske, G. K. & Fedorenko, V. A. (1998). Two mantle sources, two plumbing systems: tholeiitic and alkaline magmatism of the Maymecha River basin, Siberian flood volcanic province. *Contributions to Mineralogy and Petrology* **133**, 297–313.

Aucamp, A. P. H., Wolmarans, L. G. & Nethling, D. C. (1972). The Urfjell Group, a deformed (?) early Palaeozoic sedimentary sequence, Kirwanryggen, western Dronning Maud Land. In: Adie, R. J. (ed.) *Antarctic Geology and Geophysics*. Oslo: Universitetsforlaget, pp. 557–561.

Bevins, R. E., Rowbotham, G. & Robinson, D. (1991). Zeolite to prehnite–pumpellyite facies metamorphism of the late Proterozoic Zig-Zag Dal Basalt Formation, eastern North Greenland. *Lithos* **27**, 155–165.

Brewer, T. S., Hergt, J. M., Hawkesworth, C. J., Rex, D. & Storey, B. C. (1992). Coats Land dolerites and the generation of Antarctic continental flood basalts. In: Storey, B. C., Alabaster, T. & Pankhurst, R. J. (eds) *Magmatism and the Causes of Continental Break-up. Geological Society, London, Special Publications* **68**, 185–208.

Cadman, A. C., Tarney, J. & Baragar, W. R. A. (1995). Nature of mantle source contributions and the role of contamination and *in situ* crystallization in the petrogenesis of Proterozoic mafic dykes and flood basalts in Labrador. *Contributions to Mineralogy and Petrology* **122**, 213–229.

Carlson, R. W., Hunter, D. R. & Barker, F. (1983). Sm–Nd age and isotopic systematics of the bimodal suite, ancient gneiss complex, Swaziland. *Nature* **305**, 701–704.

Chesley, J. T. & Ruiz, J. (1998). Crust–mantle interaction in large igneous provinces: implications from the Re–Os isotope systematics of the Columbia River flood basalts. *Earth and Planetary Science Letters* **154**, 1–11.

Corner, B. (1994). Geological evolution of western Dronning Maud Land within a Gondwana framework: geophysics subprogramme. *Final project report to SACAR*. Department of Geophysics, Witwatersrand University, South Africa, 21 pp.

Cox, K. G. (1978). Flood basalts, subduction, and the break-up of Gondwanaland. *Nature* **274**, 47–49.

Cox, K. G. (1980). A model of flood basalt vulcanism. *Journal of Petrology* **21**, 629–650.

Cox, K. G. (1988). Numerical modelling of a randomized RTF magma chamber: a comparison with continental flood basalt sequences. *Journal of Petrology* **29**, 681–698.

Cox, K. G. (1989). The role of mantle plumes in the development of continental drainage patterns. *Nature* **342**, 873–877.

Cox, K. G. (1992). Karoo igneous activity, and the early stages of the break-up of Gondwnanaland. In: Storey, B. C., Alabaster, T. & Pankhurst, R. J. (eds) *Magmatism and the Causes of Continental Break-up*. *Geological Society, London, Special Publications* **68**, 137–148.

Cox, K. G. (1993). Continental magmatic underplating. In: Cox, K. G., McKenzie, D. P. & White, R. S. (eds) *Melting and Melt Movement in the Earth*. Oxford: Oxford University Press, pp. 155–166.

Cox, K. G., MacDonald, R. & Hornung, G. (1967). Geochemical and petrographic provinces in the Karoo basalts of southern Africa. *American Mineralogist* **52**, 1451–1474.

Dalziel, I. W. D, Lawver, L. A. & Murphy, J. B. (1999). Plumes, orogenies, supercontinental fragmentation and ice sheets. In: *8th International Symposium on Antarctic Earth Sciences*. *Conference Abstracts*. Wellington: The Royal Society of New Zealand, 78 pp.

DePaolo, D. J. (1981*a*). Neodymium isotopes in the Colorado Front range and crust–mantle evolution in the Proterozoic. *Nature* **291**, 193–196.

DePaolo, D. J. (1981*b*). Trace element and isotopic effects of combined wallrock assimilation and fractional crystallization. *Earth and Planetary Science Letters* **53**, 189–202.

Devey, C. W. & Cox, K. G. (1987). Relationships between crustal contamination and crystallisation in continental flood basalt magmas with special reference to the Deccan Traps of the Western Ghats, India. *Earth and Planetary Science Letters* **84**, 59–68.

Duncan, A. R. (1987). The Karoo igneous province—a problem area for inferring tectonic setting from basalt geochemistry. *Journal of Volcanology and Geothermal Research* **32**, 13–34.

Duncan, A. R., Erlank, A. J. & Marsh, J. S. (1984). Geochemistry of the Karoo igneous province. In: Erlank, A. J. (ed.) *Petrogenesis of the Volcanic Rocks of the Karoo Province. Geological Society of South Africa, Special Publications* **13**, 355–388.

Duncan, A. R., Armstrong, R. A., Erlank, A. J., Marsh, J. S. & Watkins, R. T. (1990). MORB-related dolerites associated with the final phases of Karoo flood basalt volcanism in southern Africa. In: Parker, A. J., Rickwood, P. C. & Tucker, D. H. (eds) *Mafic Dykes and Emplacement Mechanisms*. Rotterdam: Balkema, pp. 119–129.

Duncan, R. A., Hooper, P. R., Rehacek, J., Marsh, J. S. & Duncan, A. R. (1997). The timing and duration of the Karoo igneous event, southern Gondwana. *Journal of Geophysical Research* **102**, 18127–18138.

du Toit, A. L. (1937). *Our Wandering Continents, an Hypothesis of Continental Drifting*. Edinburgh: Oliver and Boyd.

Ebinger, C. J. & Sleep, N. H. (1998). Cenozoic magmatism throughout east Africa resulting from impact of a single plume. *Nature* **395**, 788–791.

Ellam, R. M. & Cox, K. G. (1989). A Proterozoic lithospheric source for Karoo magmatism: evidence from the Nuanetsi picrites. *Earth and Planetary Science Letters* **92**, 207–218.

Ellam, R. M. & Cox, K. G. (1991). An interpretation of Karoo picrite basalts in terms of interaction between asthenospheric magmas and the mantle lithosphere. *Earth and Planetary Science Letters* **105**, 330–342.

Ellam, R. M., Carlson, R. W. & Shirley, S. B. (1992). Evidence from Re–Os isotopes for plume–lithosphere mixing in Karoo flood basalt genesis. *Nature* **359**, 718–721.

Elliot, D. H. (1990). Triassic–Early Cretaceous evolution of Antarctica. In: Thomson, M. R. A., Crame, J. A. & Thomson, J. W. (eds) *Geological Evolution of Antarctica*. Cambridge: Cambridge University Press, pp. 541–548.

Elliot, D. H., Fleming, T. H., Kyle, P. R. & Foland, K. A. (1999). Long-distance transportation of magmas in the Jurassic Ferrar Large Igneous Province, Antarctica. *Earth and Planetary Science Letters* **167**, 89–104.

Erlank, A. J. (ed.) (1984). *Petrogenesis of the Volcanic Rocks of the Karoo Province*. *Geological Society of South Africa, Special Publications* **13**.

Erlank, A. J., Duncan, A. R., Marsh, J. S., Sweeney, R. J., Hawkesworth, C. J., Milner, S. C., Miller, R. McG. & Rogers, N. W. (1988). A laterally extensive geochemical discontinuity in the subcontinental Gondwana lithosphere. In: *Geochemical Evolution of the Continental Crust, Conference Abstracts*, Brazil, pp. 1–10.

Farrow, D. J., Harmer, R. E., Hunter, D. R. & Eglington, D. M. (1990). Rb–Sr and Pb–Pb dating of the Anhalt leucotonalite, northern Natal. *South African Journal of Geology* **93**, 696–701.

Faure, G., Bowman, J. R. & Elliot, D. H. (1979). The initial $^{87}Sr/^{86}Sr$ ratios of the Kirwan volcanics of Dronning Maud Land: comparison with the Kirkpatrick Basalt, Transantarctic Mountains. *Chemical Geology* **26**, 77–90.

Fleming, T. H., Foland, K. A. & Elliot, D. H. (1995). Isotopic and chemical constraints on the crustal evolution and source signature of Ferrar magmas, north Victoria Land, Antarctica. *Contributions to Mineralogy and Petrology* **121**, 217–236.

Foland, K. A., Gibb, F. G. F. & Henderson, C. M. B. (1997). The Shiant Main Sill: Nd and Sr isotopes tell a tale of two magmas and sub-solidus alteration. *Basic Science and Engineering* **1**, 1089–1095.

Foley, S. (1992). Vein-plus-wall-rock melting mechanisms in the lithosphere and the origin of potassic alkaline magmas. *Lithos* **28**, 435–454.

Furnes, H. & Mitchell, J. G. (1978). Age relationships of Mesozoic basalt lava and dykes in Vestfjella, Dronning Maud Land, Antarctica. *Norsk Polarinstitutt, Skrifter* **169**, 45–68.

Furnes, H., El-Sayed, M. M., Khalil, S. O. & Hassanen, M. A. (1996). Pan-African magmatism in the Wadi El-Imra district, Central Eastern Desert, Egypt: geochemistry and tectonic environment. *Journal of the Geological Society, London* **153**, 705–718.

Furnes, H., Neumann, E.-R. & Sundvoll, B. (1982). Petrology and geochemistry of Jurassic basalt dikes from Vestfjella, Dronning Maud Land, Antarctica. *Lithos* **15**, 295–304.

Furnes, H., Vad, E., Austrheim, H., Mitchell, J. G. & Garmann, L. B. (1987). Geochemistry of basalt lavas from Vestfjella and adjacent areas, Dronning Maud Land, Antarctica. *Lithos* **20**, 337–356.

Gallagher, K. & Hawkesworth, C. J. (1992). Dehydration melting and the generation of continental flood basalts. *Nature* **358**, 57–59.

Grantham, G. H. (1996). Aspects of Jurassic magmatism and faulting in western Dronning Maud Land, Antarctica: implications for Gondwana break-up. In: Storey, B. C., King, E. C. & Livermore, R. A. (eds) *Weddell Sea Tectonics and Gondwana Break-up*. *Geological Society, London, Special Publications* **108**, 63–73.

Grantham, G. H. & Hunter, D. R. (1991). The timing and nature of faulting and jointing adjacent to the Pencksökket, western Dronning Maud Land, Antarctica. In: Thomson, M. R. A., Crame, J. A. & Thomson, J. W. (eds) *Geological Evolution of Antarctica*. Cambridge: Cambridge Univesrity Press, pp. 47–51.

Griffiths, R. S. & Campbell, I. H. (1991). Interaction of mantle plume heads with the earth surface and onset of small-scale convection. *Journal of Geophysical Research* **91**, 18295–18310.

Groenewald, P. M., Moyes, A. B., Grantham, G. H. & Krynauw, J. R. (1995). East Antarctic crustal evolution: geological constraints and modelling in western Dronning Maud Land. *Precambrian Research* **75**, 231–250.

Haapala, I. & Rämö, O. T. (1992). Tectonic setting and origin of the Proterozoic rapakivi granites of southeastern Fennoscandia. *Transactions of the Royal Society of Edinburgh: Earth Sciences* **83**, 165–171.

Halpern, M. (1970). Rubidium–strontium date of possibly 3 billion years for a granitic rock from Antarctica. *Science* **169**, 977–978.

Harris, C. & Erlank, A. J. (1992). The production of large-volume, low-$\delta^{18}O$ rhyolites during the rifting of Africa and Antarctica: the Lebombo Monocline, southern Africa. *Geochimica et Cosmochimica Acta* **56**, 3561–3570.

Harris, C. & Grantham, G. H. (1993). Geology and petrogenesis of the Straumsvola nepheline syenite complex, Dronning Maud Land, Antarctica. *Geological Magazine* **130**, 513–532.

Harris, C., Marsh, J. S., Duncan, A. R. & Erlank, A. J. (1990). The petrogenesis of the Kirwan Basalts of Dronning Maud Land, Antarctica. *Journal of Petrology* **31**, 341–369.

Harris, C., Watters, B. R. & Groenewald, P. B. (1991). Geochemistry of the Mesozoic regional basic dykes of western Dronning Maud Land, Antarctica. *Contributions to Mineralogy and Petrology* **107**, 100–111.

Hawkesworth, C. J., Marsh, J. S., Duncan, A. R., Erlank, A. J. & Norry, M. J. (1984). The role of continental lithosphere in the generation of the Karoo volcanic rocks: evidence from combined Nd- and Sr-isotope studies. In: Erlank, A. J. (ed.) *Petrogenesis of the Volcanic Rocks of the Karoo Province. Geological Society of South Africa, Special Publications* **13**, 341–354.

Hergt, J. M., Peate, D. W. & Hawkesworth, C. J. (1991). The petrogenesis of Mesozoic Gondwana low-Ti flood basalts. *Earth and Planetary Science Letters* **105**, 134–148.

Hjelle, A. & Winsnes, T. (1972). The sedimentary and volcanic sequence of Vestfjella, Dronning Maud Land. In: Adie, R. J. (ed.) *Antarctic Geology and Geophysics*. Oslo: Universitetsforlaget, pp. 539–547.

Hungeling, A. & Thyssen, F. (1991). Reflection seismic measurements in western Neuschwabenland. In: Thomson, M. R. A., Crame, J. A. & Thomson, J. W. (eds) *Geological Evolution of Antarctica*. Cambridge: Cambridge University Press, pp. 549–555.

Hunter, D. R., Smith, R. G. & Sleigh, D. W. W. (1992). Geochemical studies of Archaean granitoid rocks in the Southeastern Kaapvaal Province: implications for crustal development. *Journal of South African Earth Sciences* **15**, 127–151.

Huppert, H. E. & Sparks, R. S. J. (1988). The generation of granitic magmas by intrusion of basalt into continental crust. *Journal of Petrology* **29**, 599–624.

Jacobs, J., Thomas, R. J. & Weber, K. (1993). Accretion and indentation tectonics at the southern edge of the Kaapvaal craton during Kibaran (Grenville) orogeny. *Geology* **21**, 203–206.

Johnson, D. M., Hooper, P. R. & Conrey, R. M. (1999). XRF analysis of rocks and minerals for major and trace elements on a single low dilution Li-tetraborate fused bead. *Advances in X-ray Analysis* **41**, 843–867.

Knaack, C., Cornelius, S. & Hooper, P. (1994). *Trace element analyses of rocks and minerals by ICP-MS*. Pullman: Department of Geology, Washington State University.

Konzett, J., Armstrong, R. A., Sweeney, R. J. & Compston, W. (1998). The timing of MARID metasomatism in the Kaapvaal mantle: an ion probe study of zircons from MARID xenoliths. *Earth and Planetary Science Letters* **160**, 133–145.

Kramers, J. D., Roddick, J. C. M. & Dawson, J. B. (1983). Trace element and isotope studies on veined, metasomatic and 'MARID' xenoliths from Bulfontein, South Africa. *Earth and Planetary Science Letters* **65**, 90–106.

Landoll, J. D., Foland, K. A. & Henderson, C. M. B. (1994). Nd isotopes demonstrate the role of contamination in the formation of coexisting quartz and nepheline syenites at the Abu Khruq Complex, Egypt. *Contributions to Mineralogy and Petrology* **117**, 305–329.

Larsen, L. M. & Rex, D. C. (1992). A review of the 2500 Ma span of alkaline–ultramafic, potassic and carbonatitic magmatism in West Greenland. *Lithos* **28**, 367–402.

Lawver, L. A. & Scotese, C. R. (1987). A revised reconstruction of Gondwanaland. In: McKenzie, G. D. (ed.) *Gondwana Six: Structure, Tectonics, and Geophysics*. Washington, DC: American Geophysical Union, pp. 17–23.

LeCheminant, A. N. & Heaman, L. M. (1989). Mackenzie igneous events, Canada: Middle Proterozoic hotspot magmatism associated with ocean opening. *Earth and Planetary Science Letters* **96**, 38–48.

Leitch, A. M., Davies, G. F. & Wells, M. (1998). A plume head melting under a rifting margin. *Earth and Planetary Science Letters* **161**, 161–177.

Le Roex, A. P., Dick, H. J. & Fisher, R. L. (1989). Petrology and geochemistry of MORB from 25°E to 46°E along the Southwest Indian Ridge: evidence for contrasting styles of mantle enrichment. *Journal of Petrology* **30**, 947–986.

Luttinen, A. V. & Siivola, J. U. (1997). Geochemical characteristics of Mesozoic lavas and dikes from Vestfjella, Dronning Maud Land: recognition of three distinct chemical types. In: Ricci, C. A. (ed.) *The Antarctic Region: Geological Evolution and Processes*. Siena: Terra Antarctica Publications, pp. 495–503.

Luttinen, A. V., Rämö, O. T. & Huhma, H. (1998). Nd and Sr isotopic and trace element composition of a Mesozoic CFB suite from Dronning Maud Land, Antarctica: implications for lithosphere and asthenosphere contributions to Karoo magmatism. *Geochimica et Cosmochimica Acta* **62**, 2701–2714.

Marsh, J. S. (1987). Basalt geochemistry and tectonic discrimination with continental flood basalt provinces. *Journal of Volcanology and Geothermal Research* **32**, 35–49.

Marsh, P. D. (1991). Major fracture trends near the western margin of East Antarctica. In: Thomson, M. R. A., Crame, J. A. & Thomson, J. W. (eds) *Geological Evolution of Antarctica*. Cambridge: Cambridge University Press, pp. 113–116.

Martin, H. (1987). Petrogenesis of Archaean trondhjemites, tonalites, and granodiorites from eastern Finland: major and trace element geochemistry. *Journal of Petrology* **28**, 921–953.

Martin, A. K. & Hartnady, C. J. (1986). Plate tectonic development of the south west Indian Ocean: a revised reconstruction of east Antarctica and Africa. *Journal of Geophysical Research* **91**, 4767–4786.

McKenzie, D. (1989). Some remarks on the movement of small melt fractions in the mantle. *Earth and Planetary Science Letters* **95**, 53–72.

Menzies, M. A. (1990). Archean, Proterozoic, and Phanerozoic lithospheres. In: Menzies, M. A. (ed.) *Continental Mantle. Monograph in Geology and Geophysics Number 16*. Oxford: Oxford University Press, pp. 67–86.

Menzies, M. A. & Murthy, V. M. (1980). Enriched mantle: Nd and Sr isotopes in diopsides from kimberlite nodules. *Nature* **283**, 634–636.

Morris, P. A. (1984). MAGFRAC: a basic program for least-squares approximation of fractional crystallization. *Computers and Geosciences* **10**, 437–444.

Moyes, A. B., Barton, J. M., Jr & Groenewald, P. B. (1993). Late Proterozoic to Early Palaeozoic tectonism in Dronning Maud Land, Antarctica: supercontinental fragmentation and amalgamation. *Journal of the Geological Society, London* **150**, 833–842.

Murphy, J. B., Oppliger, G. L., Brimhall, G. H., Jr & Hynes, A. (1998). Plume-modified orogeny: an example from the western United States. *Geology* **26**, 731–734.

O'Brien, H. E., Irving, A. J. & McCallum, I. S. (1991). Eocene potassic magmatism in the Highwood Mountains, Montana: petrology, geochemistry, and tectonic implications. *Journal of Geophysical Research* **96**, 13237–13260.

O'Hara, M. J. (1977). Geochemical evolution during fractional crystallization of a periodically refilled magma chamber. *Nature* **266**, 503–507.

Pearce, J. A. & Cann, J. R. (1973). Tectonic setting of basic volcanic rocks determined using trace element analyses. *Earth and Planetary Science Letters* **19**, 290–300.

Pearce, J. A. & Peate, D. W. (1995). Tectonic implications of the composition of volcanic arc magmas. *Annual Review of Earth and Planetary Sciences* **23**, 251–285.

Pearce, J. A., Baker, P. E., Harvey, P. K. & Luff, I. W. (1995). Geochemical evidence for subduction fluxes, mantle melting and fractional crystallization beneath the South Sandwich Island Arc. *Journal of Petrology* **36**, 1073–1109.

Pearson, D. G., Carlson, R. W., Shirley, S. B., Boyd, F. R. & Nixon, P. H. (1995). Stabilization of Archean lithospheric mantle: a Re–Os isotope study of peridotite xenoliths from the Kaapvaal craton. *Earth and Planetary Science Letters* **134**, 341–357.

Peng, Z. X., Mahoney, J., Hooper, P., Harris, C. & Beane, J. (1994). A role for lower continental crust in flood basalt genesis? Isotopic and incompatible element study of the lower six formations of the western Deccan Traps. *Geochimica et Cosmochimica Acta* **58**, 267–288.

Peters, M., Haverkamp, B., Emmermann, R., Kohnen, H. & Weber, K. (1991). Palaeomagnetism, K–Ar dating and geodynamic setting of igneous rocks in western and central Neuschwabenland, Antarctica. In: Thomson, M. R. A., Crame, J. A. & Thomson, J. W. (eds) *Geological Evolution of Antarctica.* Cambridge: Cambridge University Press, pp. 549–555.

Pin, C., Briot, D., Bassin, C. & Poitrasson, F. (1994). Concomitant separation of strontium and samarium–neodymium for isotope analyses in silicate samples, based on specific extraction chromatography. *Analytica Chimica Acta* **298**, 209–217.

Räisänen, M. H., Vuori, S. K., Luttinen, A. V. & Siivola, J. U. (1999). Observations on the Jurassic Utpostane and Muren gabbroic intrusions of Vestfjella, western Dronning Maud Land. In: *8th International Symposium on Antarctic Earth Sciences. Conference Abstracts.* Wellington: The Royal Society of New Zealand, 257 pp.

Rämö, O. T. (1991). Petrogenesis of the Proterozoic rapakivi granites and related basic rocks of southeastern Fennoscandia: Nd and Pb isotopic and general geochemical constraints. *Geological Survey of Finland Bulletin* **355**, 161 pp.

Richard, P., Shimizu, N. & Allègre, C. J. (1976). $^{143}Nd/^{144}Nd$, a natural tracer: an application to oceanic basalts. *Earth and Planetary Science Letters* **31**, 269–278.

Richardson, S. H., Gurney, J. J., Erlank, A. J. & Harris, J. W. (1984). Origin of diamonds in old enriched mantle. *Nature* **310**, 198–202.

Rock, N. M. S. (1991). *Lamprophyres.* Glasgow: Blackie.

Rollinson, H. R. (1993). *Using Geochemical Data: Evaluation, Presentation, Interpretation.* Harlow, UK: Longman.

Rudnick, R. L. & Fountain, D. M. (1995). Nature and composition of the continental crust: a lower crustal perspective. *Reviews of Geophysics* **33**, 267–309.

Ruotoistenmäki, T. & Lehtimäki, J. (1997). Analysis of bedrock geology and thermal gradients using geophysical ground measurements on glaciated terrain in Queen Maud Land, Antarctica. In: Ricci, C. A. (ed.) *The Antarctic Region: Geological Evolution and Processes.* Siena: Terra Antarctica Publications, pp. 1149–1152.

Salonsaari, P. T. (1995). Hybridization in the subvolcanic Jaala–Iitti Complex and its petrogenetic relation to rapakivi granites and associated mafic rocks of southeastern Finland. *Bulletin of the Geological Society of Finland* **67/1b**, 1–104.

Saunders, A. D., Storey, M., Kent, R. W. & Norry, M. J. (1992). Consequences of plume–lithosphere interactions. In: Storey, B. C., Alabaster, T. & Pankhurst, R. J. (eds) *Magmatism and the Causes of Continental Break-up. Geological Society, London, Special Publications* **68**, 41–60.

Self, S., Thordarson, Th., Keszthelyi, L., Walker, G. P. L., Hon, K., Murphy, M. T., Long, P. & Finnemore, S. (1996). A new model for the emplacement of Columbia River basalts as large, inflated pahoehoe lava flow fields. *Geophysical Research Letters* **23**, 2689–2692.

Spaeth, G. (1987). Aspects of the structural evolution and magmatism in western New Schwabenland, Antarctica. In: McKenzie, G. D. (ed.) *Gondwana Six: Structure, Tectonics and Geophysics*. Washington, DC: American Geophysical Union, pp. 295–307.

Storey, B. C., Alabaster, T., Hole, M. J., Pankhurst, R. J. & Wever, H. E. (1992). Role of subduction–plate boundary forces during the initial stages of Gondwana break-up: evidence from the proto-Pacific margin of Antarctica. In: Storey, B. C., Alabaster, T. & Pankhurst, R. J. (eds) *Magmatism and the Causes of Continental Break-up. Geological Society, London, Special Publications* **68**, 149–163.

Sun, S. S. & McDonough, W. F. (1989. Chemical and isotopic systematics of oceanic basalts: implications for mantle composition and processes. In: Saunders, A. D. & Norry, M. J. (eds) *Magmatism in Ocean Basins. Geological Society, London, Special Publications* **42**, 313–345.

Sweeney, R. J. & Watkeys, M. K. (1990). A possible link between Mesozoic lithospheric architecture and Gondwana flood basalts. *Journal of African Earth Science* **10**, 707–716.

Sweeney, R. J., Duncan, A. R. & Erlank, A. J. (1994). Geochemistry and petrogenesis of Central Lebombo basalts of the Karoo Igneous Province. *Journal of Petrology* **35**, 95–125.

Tatsumi, Y., Hamilton, D. L. & Nesbitt, R. W. (1986). Chemical characteristics of fluid phase released from a subducted lithosphere and origin of arc magmas: evidence from high-pressure experiments and natural rocks. *Journal of Volcanology and Geothermal Research* **29**, 293–309.

Thompson, R. N. & Gibson, S. A. (1991). Subcontinental mantle plumes, hotspots and pre-existing thinspots. *Journal of the Geological Society, London* **148**, 973–977.

Turner, S. & Hawkesworth, C. J. (1995). The nature of the sub-continental mantle: constraints from the major-element composition of continental flood basalts. *Chemical Geology* **120**, 295–314.

Walker, R. J., Carlson, R. W., Shirley, S. B. & Boyd, F. R. (1989). Osmium, strontium, neodymium, and lead isotope systematics of southern African peridotite xenoliths: implications for the chemical evolution of subcontinental mantle. *Geochimica et Cosmochimica Acta* **53**, 1583–1595.

Waters, F. G. (1987). A suggested origin of MARID xenoliths in kimberlites by high pressure crystallization of an ultrapotassic rock such as lamproite. *Contributions to Mineralogy and Petrology* **95**, 523–533.

White, R. S. (1992). Magmatism during and after continental break-up. In: Storey, B. C., Alabaster, T. & Pankhurst, R. J. (eds) *Magmatism and the Causes of Continental Break-up. Geological Society, London, Special Publications* **68**, 1–16.

White, R. S. & McKenzie, D. (1989). Magmatism at rift zones: the generation of volcanic continental margins and flood basalts. *Journal of Geophysical Research* **94**, 7685–7729.

Wood, D. A., Gibson, I. L. & Thompson, R. N. (1976). Elemental mobility during zeolite facies metamorphism of the Tertiary basalts of eastern Iceland. *Contributions to Mineralogy and Petrology* **55**, 241–254.

Yoder, H. S. & Tilley, C. E. (1962). Origin of basalt magmas: an experimental study of natural and synthetic rock systems. *Journal of Petrology* **3**, 342–532.

Zindler, A. & Hart, S. R. (1986) Chemical geodynamics. *Annual Review of Earth and Planetary Sciences* **14**, 493–571.